C. P. No. 714

C. P. No. 714

MINISTRY OF AVIATION

AERONAUTICAL RESEARCH COUNCIL

CURRENT PAPERS

Flutter Tests and Calculations on an All-Moving Model Fin

By

J. K. Curran

LONDON HER MAJESTY'S STATIONERY OFFICE

1964

SEVEN SHILLINGS NET

U.D.C. No. 533.6.013.422 : 533.694.541

C.P. No. 714

July, 1963

FLUTTER TESTS AND CALCULATIONS ON AN ALL-MOVING MODEL FIN

by

J. K. Curran

SUMMARY

Low speed flutter tests have been made on an all-moving model fin to ascertain the effect of mass balance at a position on the leading edge near the root. The stiffness of the joint forming the roll axis for the model was also varied.

Good agreement is obtained between the experimental results and analytical predictions. As the stiffness at the joint is increased, allowing less freedom in roll, the flutter speed falls rapidly to a minimum, initially, and subsequently increases. Mass-balance reduces the flutter speeds and frequencies.

Calculations by the Aircraft Industry on a particular all-moving fin, which served as a basis for the model, gave the opposite effect for mass-balance, but the model did not accurately represent the chordwise flexibility of the actual fin and it is possible that the effectiveness of mass balance at the root depends on this parameter.

Replaces R.A.E. Tech.Note No. Structures 330 - A.R.C. 25,228.

CONTENTS

TABLES

ILLUSTRATIONS

1 INTRODUCTION

In recent years a greater use has been made of all-moving surfaces (tailplane and fin) for aircraft control. Experimental data on the flutter properties of all-moving surfaces is, however, scarce and a programme of low speed tests was undertaken to obtain additional information.

Theoretical investigations by the Aircraft Industry on the flutter characteristics of a particular all-moving fin showed that mass-balance on the leading edge near the root improved the flutter properties significantly. This result seemed somewhat unusual as mass balance in this position was considered unlikely to prevent coupling of the modes conducive to flutter. It was decided therefore to use this particular fin as a basis for the design of the flutter model for the low speed tests.

The manufacture of a model having detailed correspondance with the full scale structures would have required a prohibitive expenditure of time and effort and was not attempted. Instead it was assumed that the actual fin had a definable flexual axis along which the stiffness could be concentrated and this enabled a simple single spar model with a number of ribs and a covering of polyurethane foam to be used in the tests.

There was agreement in planform between the model and the actual fin and a general order of agreement in stiffness and inertia distribution, but representation was particularly lacking as regards chordwise deformation. The model, however, was considered adequate to establish flutter trends with reasonable reliability.

The inertia, stiffness and resonance characteristics of the model were measured, and subsequently low speed flutter tests were made, with and without mass balance, for different values of the stiffness of the joint forming the roll axis for the model. Flutter speeds and frequencies were also obtained by calculation and compared with the experimental values.

2 DETAILS OF THE MODEL

The model, depicted in Figs.1 and 2, consisted of a metal framework covered with polyurethane foam. A single duralumin spar provided the stiffness and a number of ribs, welded to the spar, gave the required mass distribution. The foam was shaped to conform to the aerodynamic section R.A.E. 101 with a ten per cent thickness/chord ratio.

The model had freedom in roll about an axis two inches below the root end of the spar, the amount of rotation depending on the stiffness at the joint. A system of cross springs, shown in Fig.3, formed the joint and variation of the stiffness was achieved by interchanging the springs. Mass balance could be attached to the model at the position indicated in Fig.4.

3 INERTIA, STIFFNESS AND RESONANCE TESTS

The inertia, stiffness and resonance characteristics of the model were determined both for the bare metal structure and for the covered model. The inertias were obtained by timing free oscillations and the stiffness and resonance properties relate to fixed root conditions.

The stiffnesses are presented in matrix form in Tables 1 and 2 and the points at which the deflections were measured are denoted in Figs.5 and 6. Details of the inertias are given in Table 3.

The resonant frequencies of the first five natural modes of vibration were determined by exciting the model and recording the frequencies at the peak amplitudes. At each resonant frequency the displacements were measured at the points shown in Figs.5 and 7. The results for the bare structure are given in Figs.8 to 12 and for the covered model in Figs.13 to 17. In the latter case the contours are lines of equal amplitude.

4 WIND TUNNEL TESTS

The model was tested in the R.A.E. 5 ft open jet wind tunnel and the critical flutter speeds and frequencies were determined, with and without mass balance, for increasing values of the stiffness of the joint forming the roll axis. The values ranged from 20 lb ft/rad to 455 lb ft/rad.

The effect of mass balance on the flutter properties of the model was investigated using two mass balance weights of 0.03 lb and 0.06 lb, 3% and 6% respectively of the weight of the model.

A small piezo-electric bender-type transducer, attached to the model, was used to record the acceleration response. At high wind speeds the noise of the tunnel generated a relatively high frequency acceleration response which tended to swamp the output signal from the transducer.

The results of the tests are given in Fig.18 and the layout of the transducer circuit in Fig.19.

5 CALCULATIONS

5.1 Calculated modes

The fin was regarded as divided up into 17 regions with concentrated masses. Using these discrete masses in association with the measured influence coefficient matrix (Table 2) a set of modes was calculated.

The mass distribution is presented in Table 4 and the calculated modes in Figs.20 to 24.

5.2 Flutter calculations

A quaternary flutter calculation was made on the model. The modes were, roll about an axis two inches below the root and the first three natural modes of vibration relative to fixed root conditions. The calculations involved the determination of the inertia, stiffness and aerodynamic coefficients in non-dimensional form; details of the methods used are given in Appendix 1.

The complete flutter equations were solved by the R.A.E. Twelve Degree of Freedom Electronic Flutter Simulator and the flutter speeds and frequencies for a joint stiffness range of 20 lb ft/rad to 450 lb ft/rad are presented in Fig.25.

The theoretical flutter speeds for the fixed root condition (no roll) were 320 ft/sec and 295 ft/sec with and without mass-balance respectively and the corresponding flutter frequencies were 31 c/s and 26 c/s.

6 DISCUSSION OF THE WIND TUNNEL RESULTS

The curves in Fig.18 show that mass balance reduces the flutter speeds and frequencies the larger mass causing the greater reduction.

As the stiffness of the joint, about which the model rolls, is increased, the flutter speed falls rapidly to a minimum and subsequently increases. The effect is the same with and without mass balance. The flutter frequencies increase slowly with increasing stiffness.

For the nominally fixed root condition (no roll freedom) the flutter speed and frequency for the fin, without mass balance, were 252 ft/sec and 23 c/s respectively, whereas, with mass balance (0.06 lb) the flutter speed was greater than 285 ft/sec - the maximum tunnel speed. This result indicates that mass balance is advantageous for the fixed root case. However, there is some uncertainty regarding the effectiveness of the root fixing in these particular tests and this result should be treated with reserve.

7 COMPARISON BETWEEN THEORETICAL AND EXPERIMENTAL RESULTS

7.1 Measured and calculated modes

A comparison of the measured modes (Figs.13 to 17) with those calculated (Figs.20 to 24) indicates tolerable agreement in the lower frequency range; the first two modes agree fairly well both in frequency and nodal line shape, but the third experimental mode is very similar to the fourth calculated mode. There is practically no agreement between the modes of higher order, but better agreement could undoubtedly be obtained by increasing the number of points for influence coefficient measurements and the number of regions for mass distribution.

7.2 Wind tunnel results and theoretical predictions

The experimental and theoretical curves are compared in Fig.25, the first diagram relating to the flutter speeds and the second to the flutter frequencies.

The flutter speed curves show that, with and without mass balance, there is good agreement between the wind tunnel results and the calculations. The theory accurately predicts not only the effects of joint stiffness and mass balance but also the actual values of flutter speed.

The flutter frequency curves show that the effects of roll stiffness and mass balance, as determined experimentally, are substantiated by calculation, but the theoretical values are higher.

With regard to the nominally fixed root results a discrepancy occurs; the calculations show that mass balance has the same effect on flutter speed as when roll is permitted, but the experiments indicate the opposite effect. However, as mentioned in section 6, some doubt exists regarding the effectiveness of the root fixing and it is possible that the flutter speed for the fin without mass balance should have been higher than that obtained with mass balance, as indicated by calculation.

The comparison between model calculations and experiment shows that the theory is adequate for the prediction of the flutter characteristics of an all-moving surface.

At the same time it should be noted that the trends obtained for the model are at variance with those obtained from calculations on the full scale fin. However, it seems likely that chordwise flexibility is of major importance in the full scale work, and this feature was not adequately represented in the model.

8 CONCLUSIONS

(a) As the stiffness at the joint forming the roll axis is increased, allowing less freedom in roll, the flutter speed falls rapidly to a minimum initially and subsequently increases.

(b) Mass balance on the leading edge, near the root, decreases the flutter speed and frequency.

(c) Close agreement between the experimental results and calculations indicates that the theory is adequate for the prediction of the flutter characteristics of an all-moving surface in the absence of compressibility effects.

(d) Mass balance effects for the model are the opposite of those indicated by calculations for a full scale fin. The inadequate representation of the chordwise flexibility may provide an explanation for this discrepancy.

APPENDIX 1

FLUTTER CALCULATIONS

A quaternary flutter calculation was made on the model. The modes were, the roll about an axis two inches below the root and the first three natural modes of vibration of the model relative to fixed root conditions. The calculations involved the determination of the inertia, stiffness and aerodynamic coefficients in non-dimensional form.

To obtain the inertia coefficients the fin was regarded as divided into 62 concentrated masses. The coefficients were then calculated from the values of these masses and their displacements in the four modes from the relationship:-

$$a_{pq} = \frac{1}{\rho S C_r^2} \sum m f_p f_q$$

where a_{pq} = inertia coefficient

ρ = air density

S = semi span

C_r = reference chord

m = concentrated mass

f_p = displacement function in mode p

f_q = displacement function in mode q.

The displacement functions were obtained from the contour line diagrams for the first three modes and were calculated for the roll mode.

The structural stiffness coefficients were obtained from the relation:-

$$e_{pp} = a_{pp} \cdot w_p^2 \frac{C_r^2}{V^2}$$

where e_{pp} is the structural stiffness coefficient

a_{pp} is the direct structural inertia

w_p is the natural frequency of mode p

V is the airspeed.

The aerodynamic coefficients were calculated using a method developed by D.E. Davies of Structures Department, R.A.E., and programmed for the Mercury computer (Programme R.A.E. 161A).

The procedure involves the selection of a number of spanwise stations with particular locations. At each station a number of displacement and upwash points are selected in the streamwise direction. Displacements at these chosen points and the slopes at the upwash points are then determined for the modes involved in the flutter calculations. These values in conjunction with values of frequency parameter and Mach Number and some model co-ordinates are used to obtain the non-dimensional aerodynamic coefficients required for the flutter matrix.

TABLE 1

Influence coefficients for the bare fin (in./lb)

	1	2	3	4	5	6	7	8	9	10	11	12
1	0.045176	-0.01195	-0.000999	-0.00127	0.000499	-0.001388	0.00025	-0.00155	-0.000399	-0.00133	-0.000986	-0.001638
2	-0.001276	0.072716	-0.000541	0.001999	-0.00022	0.002554	0.000652	0.002638	0.001699	0.002638	0.002485	0.00304
3	0.000999	-0.000555	0.007219	-0.002151	0.001361	-0.002443	0.000379	-0.002443	-0.0004999	-0.002388	-0.001471	-0.003246
4	-0.001276	0.001999	-0.00236	0.04854	-0.000499	0.006163	0.001555	0.007609	0.003096	0.008913	0.005637	0.008886
5	0.0004999	-0.000222	0.001235	-0.000444	0.00908	-0.00576	0.003136	-0.00472	0.002332	-0.002804	0.001638	-0.001721
6	-0.001402	0.0024133	-0.00236	0.006859	-0.005289	0.101049	0.004207	0.040264	0.017799	0.044013	0.030726	0.048317
7	0.00025	0.000638	0.000319	0.001555	-0.00304	0.004859	0.017674	0.004248	0.027103	0.019354	0.038487	0.035266
8	-0.001499	0.002419	-0.002388	0.007663	-0.004359	0.039596	0.003999	0.157003	0.056342	0.140647	0.10956	0.167424
9	-0.000341	0.001658	-0.0004999	0.003277	0.002541	0.017605	0.025671	0.056259	0.097523	0.10924	0.174386	0.19999
10	-0.001457	0.002943	-0.00272	0.008719	-0.002776	0.043216	0.018035	0.14062	0.120983	0.34823	0.2995	0.44346
11	-0.001	0.0025	-0.0015	0.00575	0.0015	0.02925	0.036	0.111	0.174	0.2885	0.43925	0.4755
12	-0.0015	0.0030	-0.00375	0.00875	-0.00175	0.044	0.03695	0.165	0.19225	0.42524	0.4775	1.0200

Positions 1 - 12 are indicated in Fig.5.

TABLE 2

Influence coefficients (in./lb). Model covered with Spando foam 200

	1	2	3	4	5	6	7	8	9	10	11	12	13	14	15	16	17
1	0.27200	0.28870	0.31350	0.11650	0.13750	0.17200	0.03190	0.04600	0.07000	0.00430	0.01220	0.02470	-0.00200	0.00275	0.00780	-0.00487	0.00400
2	0.28750	0.32450	0.38370	0.12170	0.15250	0.20000	0.03160	0.05230	0.08730	0.00360	0.01450	0.03500	-0.00350	0.00300	0.01100	-0.00605	0.00620
3	0.29550	0.38000	0.45500	0.13250	0.16300	0.23000	0.03185	0.05950	0.09900	0.00290	0.01580	0.03950	-0.00422	0.00330	0.01250	-0.00715	0.00820
4	0.11625	0.11750	0.13250	0.08500	0.07250	0.07950	0.02115	0.02820	0.03800	0.00400	0.00810	0.01460	-0.00190	0.00200	0.00400	-0.00240	0.00195
5	0.13375	0.15120	0.16950	0.07250	0.09500	0.11150	0.02090	0.03540	0.05610	0.00255	0.01065	0.02300	-0.00197	0.00240	0.00855	-0.00410	0.00490
6	0.16375	0.20050	0.23070	0.08000	0.11150	0.18120	0.01940	0.04460	0.08110	0.00090	0.01310	0.03600	-0.00402	0.00290	0.01300	-0.00570	0.00900
7	0.03180	0.03000	0.03315	0.02090	0.02000	0.02200	0.01000	0.01010	0.01050	0.00390	0.00390	0.00355	0.00153	0.00125	0.00090	-0.00030	-0.00010
8	0.04800	0.05310	0.05910	0.02880	0.03700	0.04490	0.01110	0.02600	0.03100	0.00170	0.00660	0.01600	-0.00110	0.00180	0.00695	-0.00240	0.00381
9	0.07260	0.08600	0.10250	0.03850	0.05730	0.08300	0.00950	0.03100	0.07050	0	0.01075	0.03310	-0.00356	0.00247	0.01405	-0.00465	0.01020
10	0.00400	0.00330	0.00285	0.00400	0.00200	0.00100	0.00400	0.00165	0	0.06350	0.00100	-0.00070	0.00344	0.00063	-0.00080	0.00262	-0.00092
11	0.01450	0.01485	0.01485	0.00810	0.01500	0.01290	0.00410	0.00705	0.01040	0.00110	0.00375	0.00760	-0.00034	0.00125	0.00400	-0.00112	0.00335
12	0.02550	0.03225	0.03900	0.01310	0.02400	0.03600	0.00370	0.01600	0.03310	-0.00083	0.00800	0.04160	-0.00282	0.00240	0.01750	-0.00297	0.01400
13	-0.00175	-0.00330	-0.0405	-0.00200	-0.00200	-0.00400	0.00134	-0.00110	-0.00290	0.00315	-0.00026	-0.00235	0.00215	0.00017	-0.00170	0.00950	-0.00162
14	0.00305	0.00280	0.03400	0.00185	0.00120	0.00260	0.00100	0.00180	0.00315	0.00046	0.00127	0.00240	0.00023	0.01450	0.00225	-0.00016	0.00225
15	0.00800	0.01115	0.01285	0.00430	0.00820	0.01390	0.00083	0.00650	0.01400	-0.00090	0.00405	0.01810	-0.00180	0.00230	0.02800	-0.00260	0.02350
16	-0.0043	-0.00505	-0.00615	-0.00285	-0.00370	-0.00600	-0.00021	-0.00230	-0.00420	0.00223	-0.00115	-0.00325	0.01045	-0.00035	-0.00290	0.03600	-0.00224
17	0.00390	0.00650	0.00730	0.00170	0.00460	0.00800	-0.00007	0.00400	0.00890	-0.00098	0.00277	0.01275	-0.00190	0.00212	0.02265	-0.00205	0.04200

Positions numbered 1 to 17 are indicated in Fig.6.

TABLE 3

Results of inertia tests

Condition	I_{roll} (lb in.^{2})	Mass (lb)
Metal framework	28.3	0.52
Covered with foam	63.5	0.98

Roll axis:- 2 in. below root end of spar and parallel to tip rib.

TABLE 4

Mass distribution

Position (As indicated in Fig.10)	Mass (lb) (Metal + foam + glue)
1	0.03454
2	0.01894
3	0.01700
4	0.06427
5	0.04411
6	0.02974
7	0.08945
8	0.05417
9	0.02913
10	0.09111
11	0.06550
12	0.03468
13	0.11813
14	0.11413
15	0.04238
16	0.10209
17	0.03524

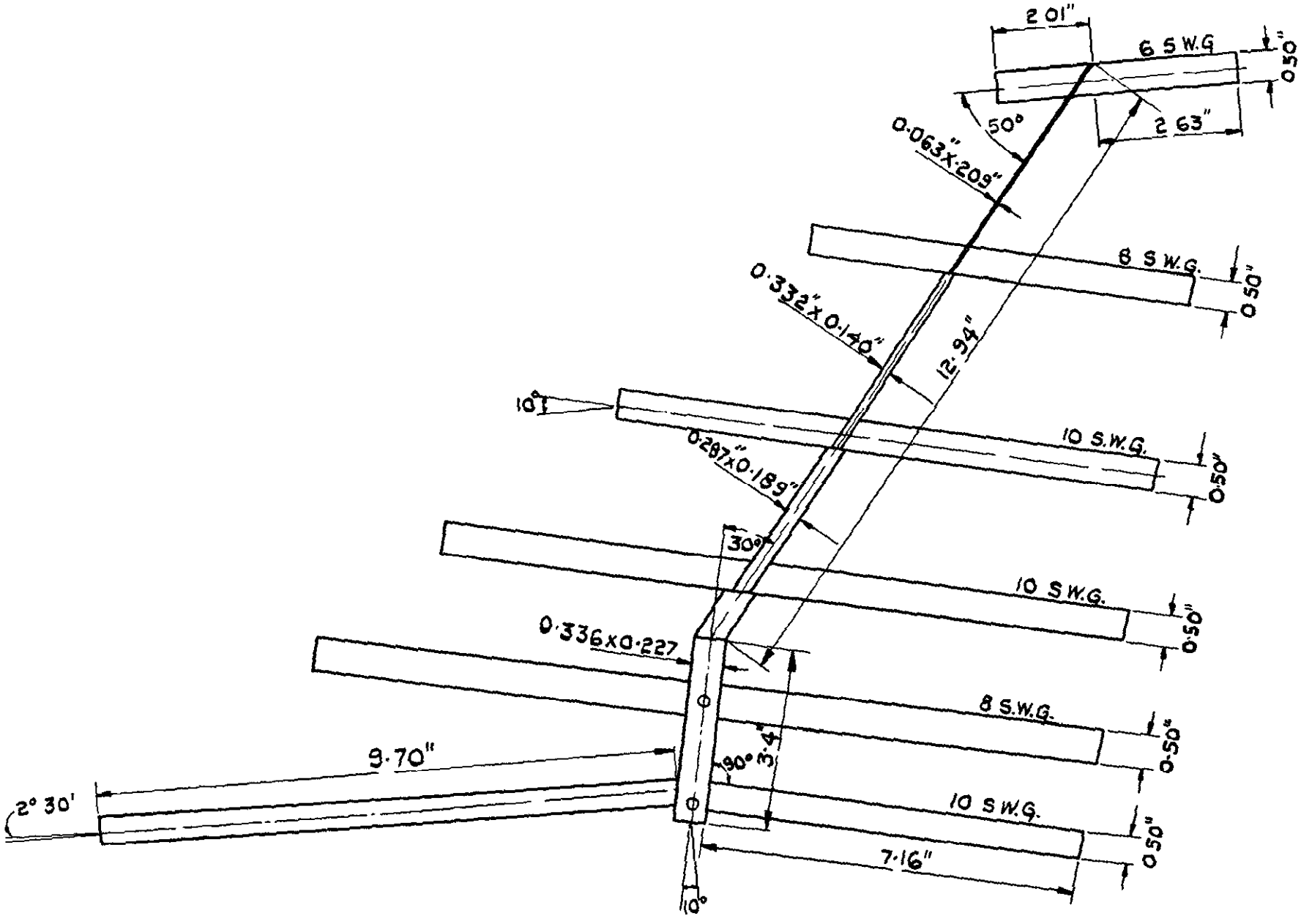

FIG. 1. DIMENSIONS OF METAL FRAMEWORK

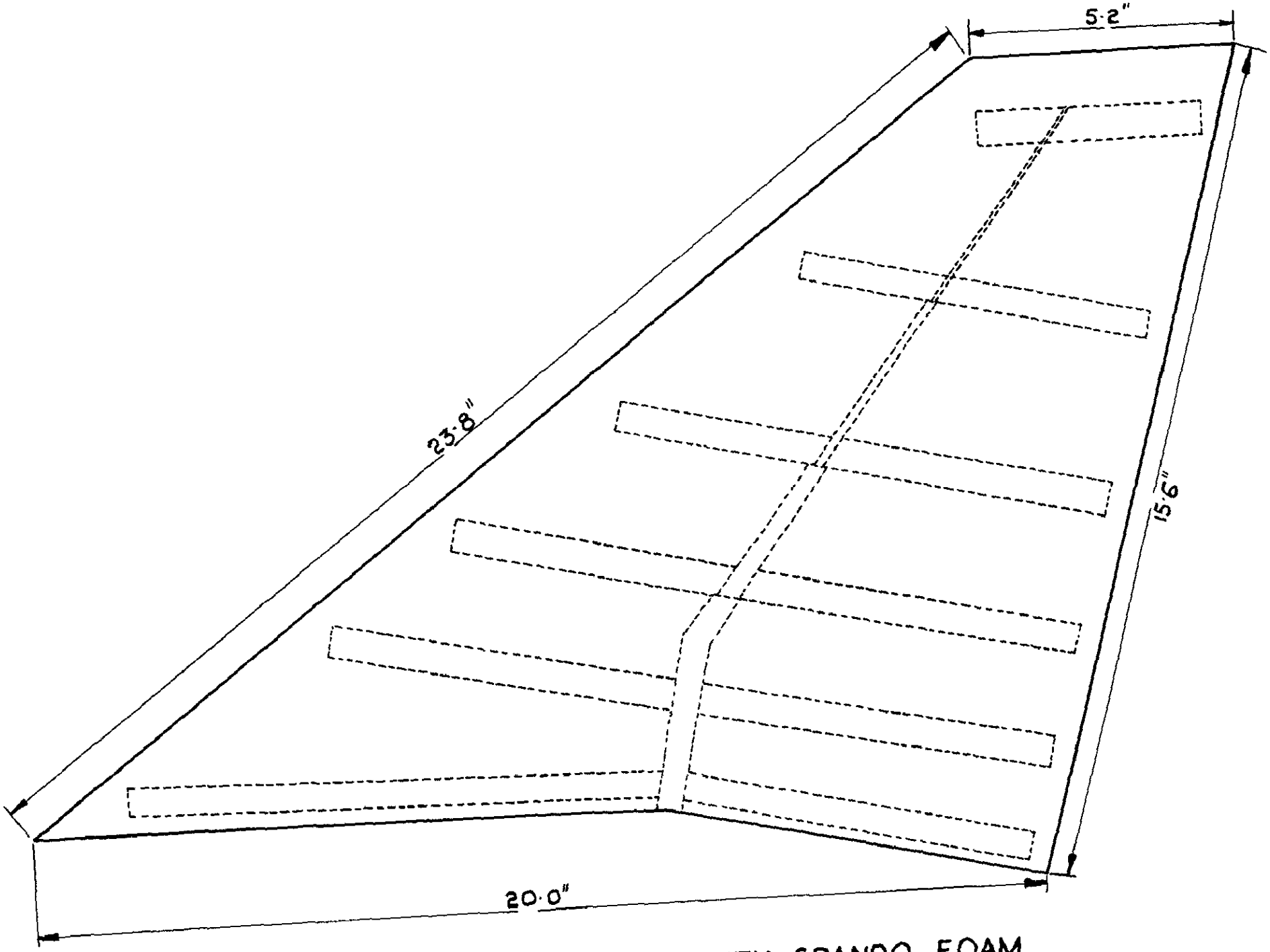

FIG. 2. MODEL COVERED WITH SPANDO FOAM.

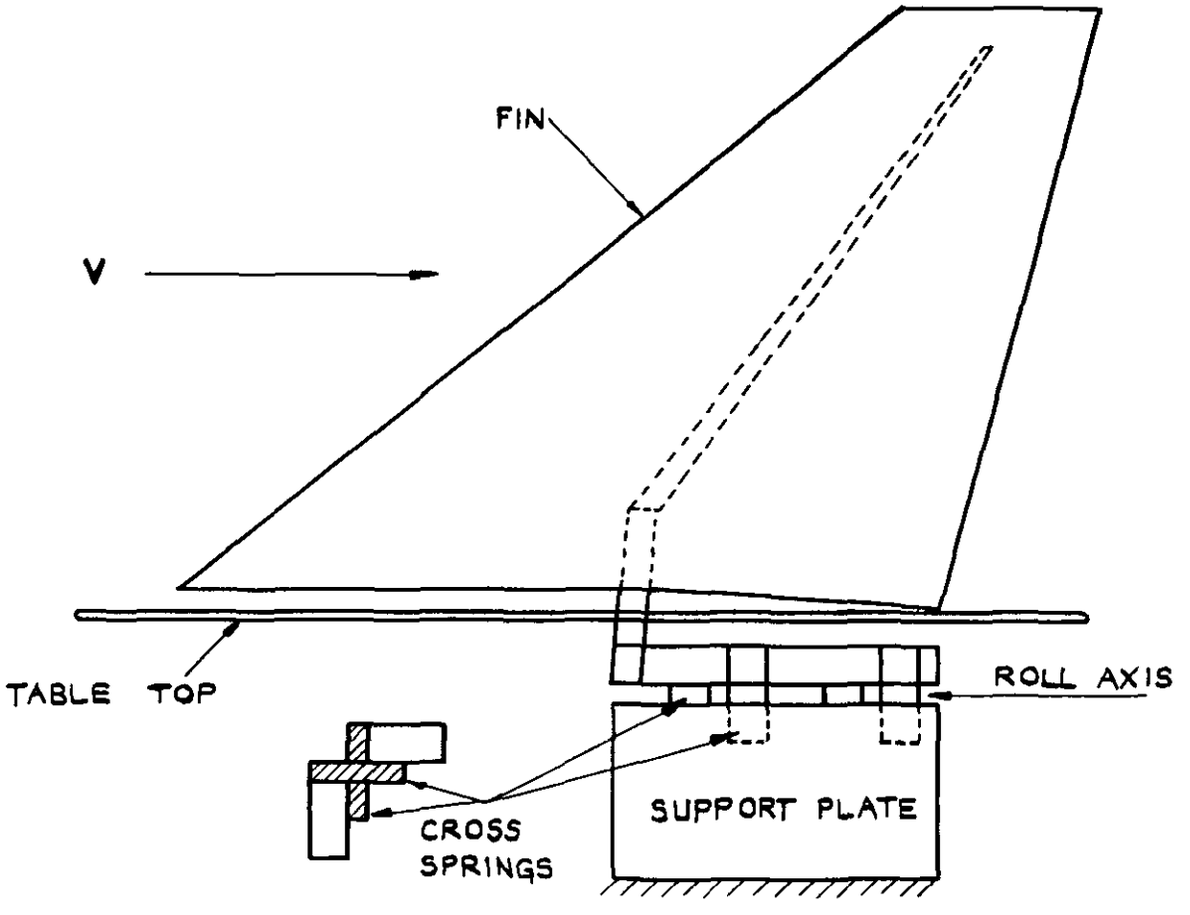

FIG. 3. FIN AND RIG.

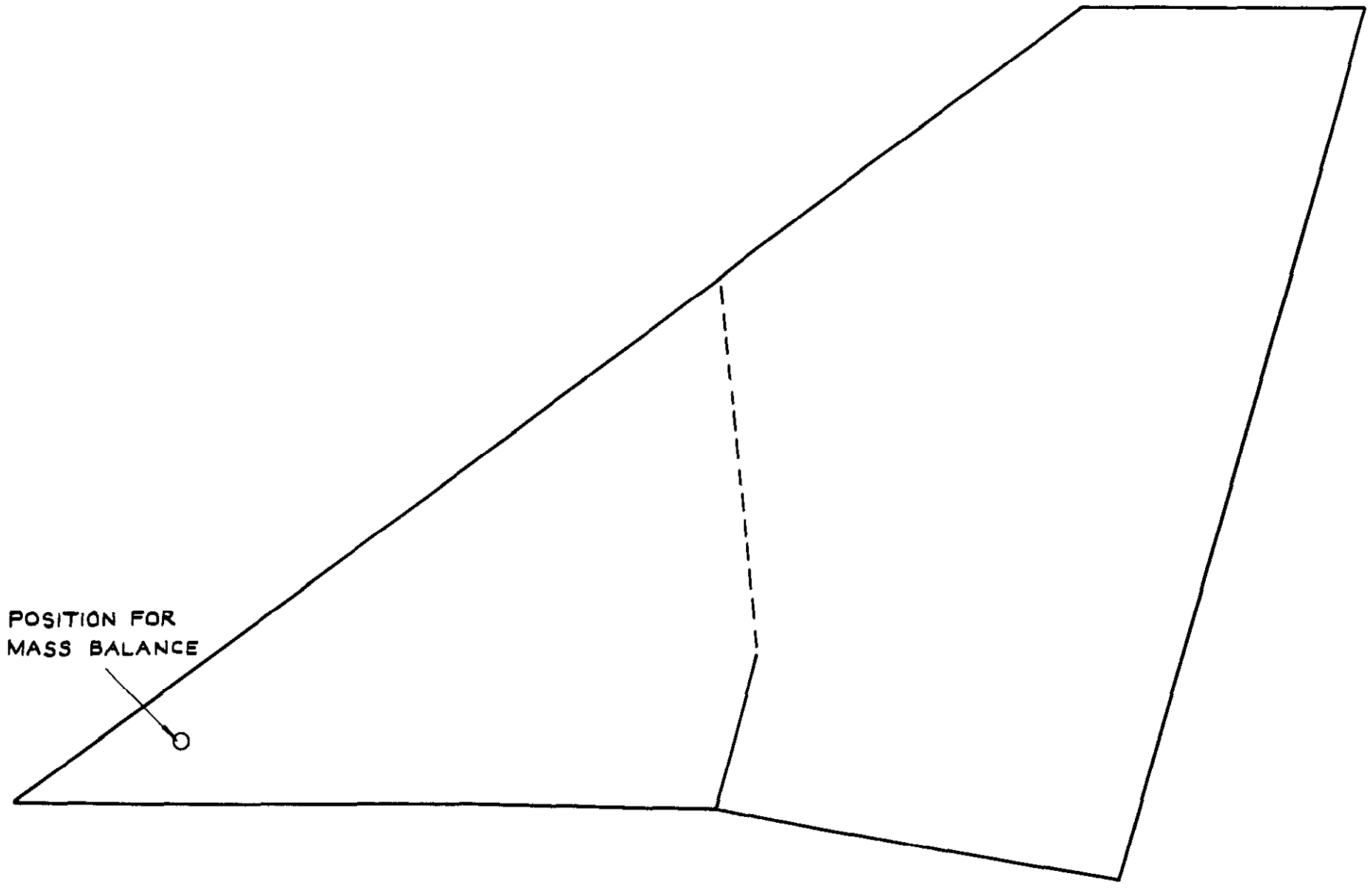

FIG. 4. APPARENT NODAL LINE AT FLUTTER.

O POINTS AT WHICH STATIC DEFLECTIONS WERE MEASURED

X POINTS AT WHICH MODES WERE MEASURED

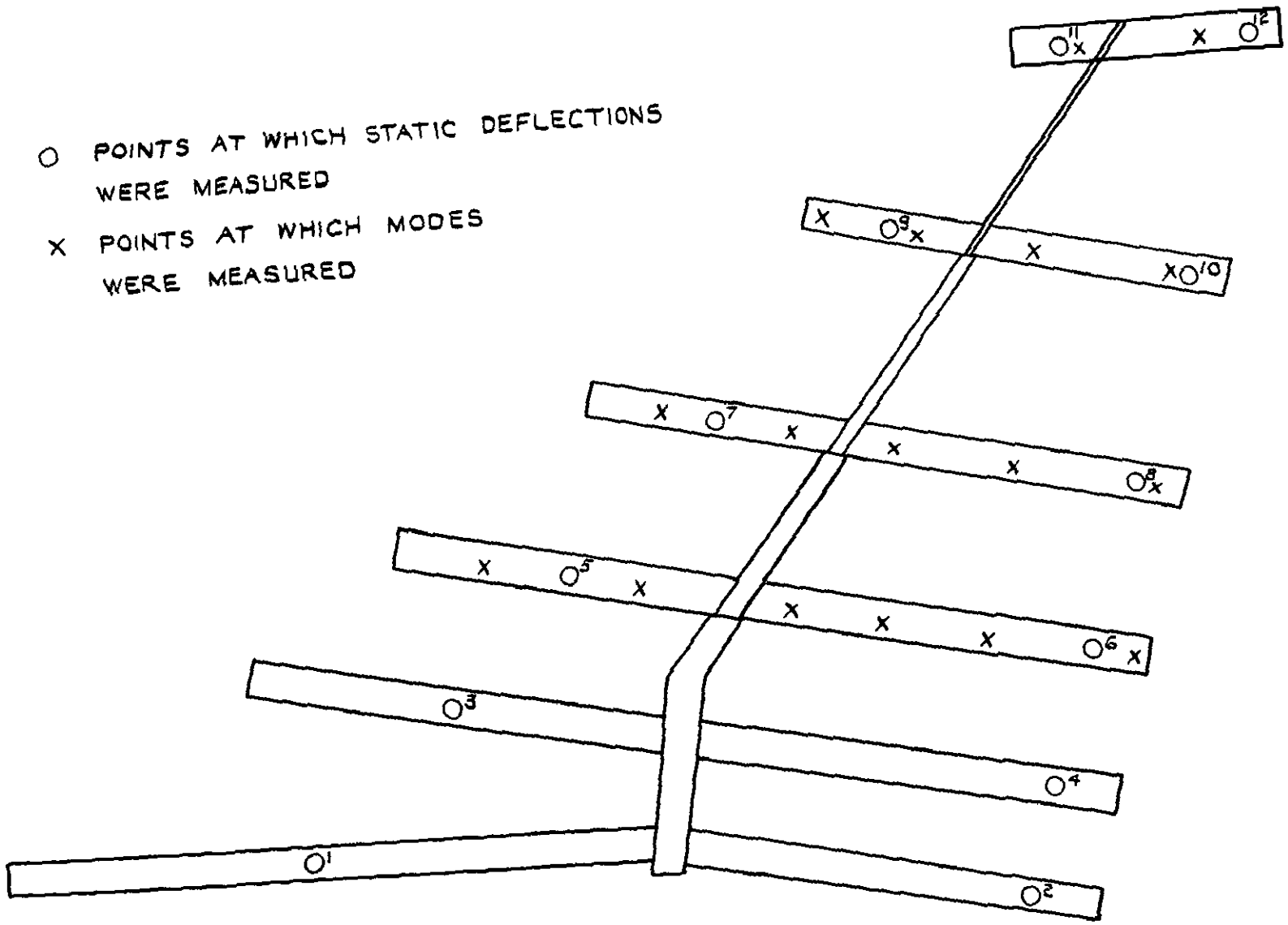

FIG. 5. MEASURING POINTS ON METAL STRUCTURE.

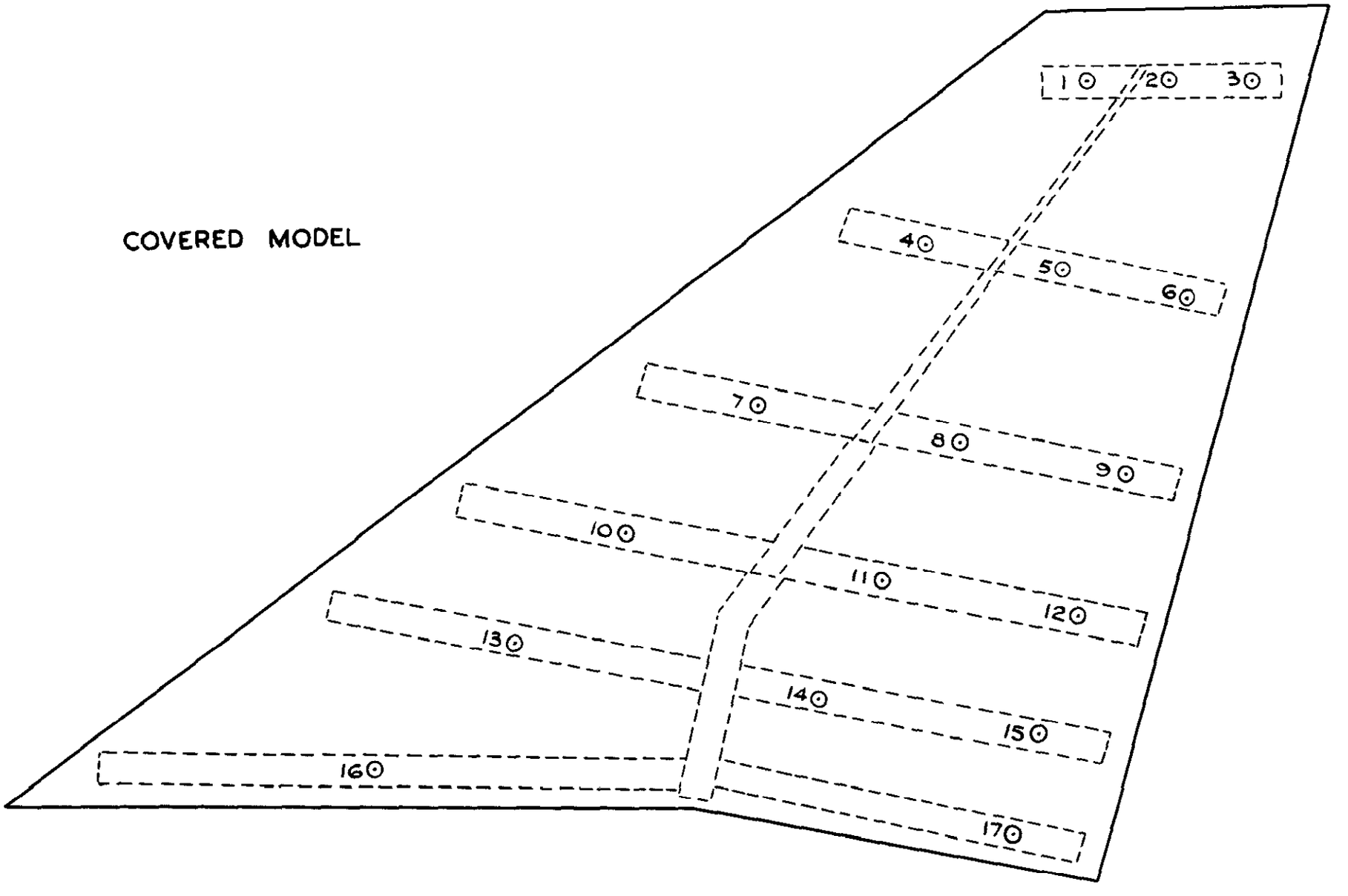

FIG. 6. POINTS AT WHICH STATIC DEFLECTIONS WERE MEASURED.

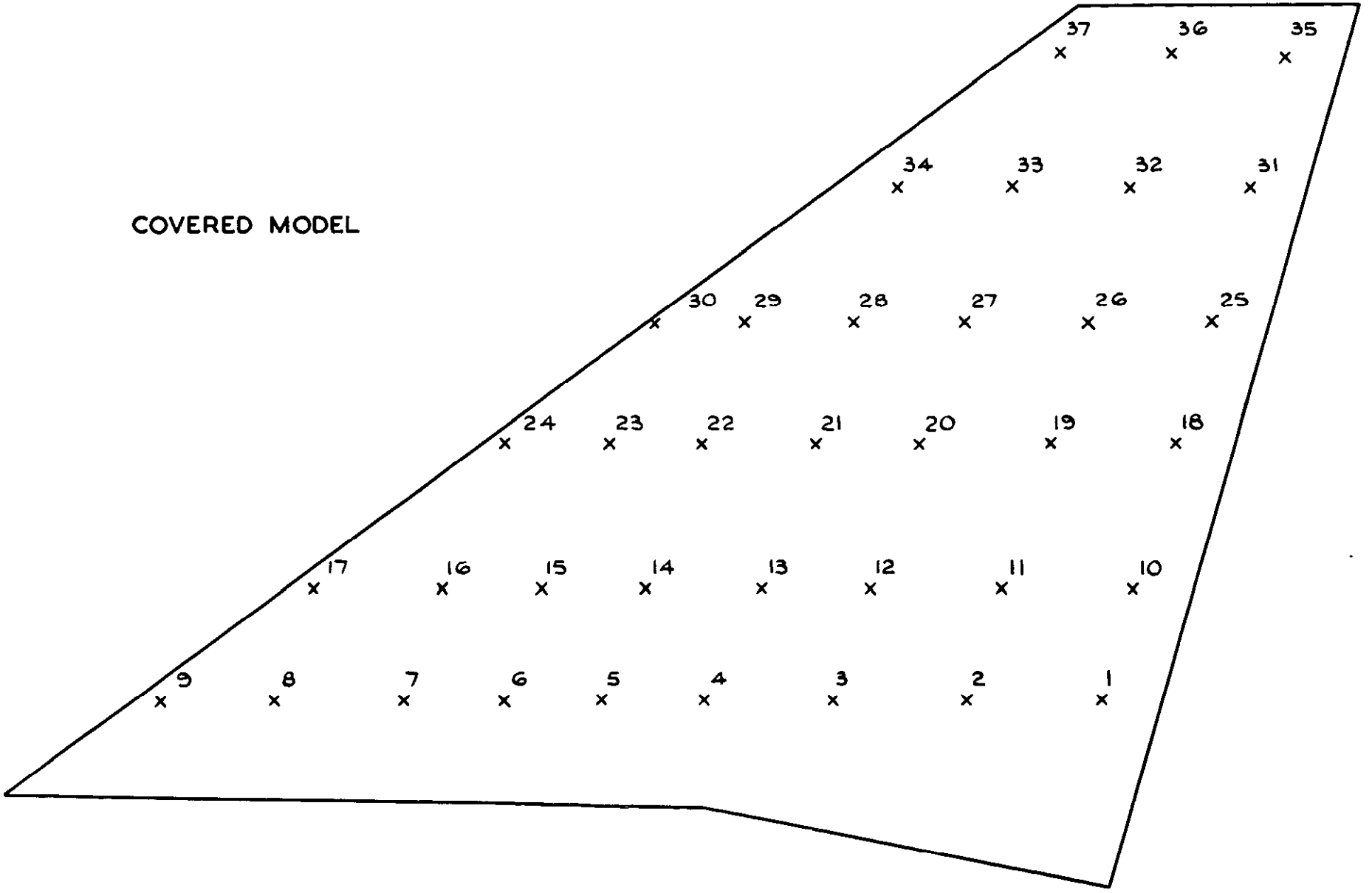

FIG. 7. POINTS AT WHICH THE MODES WERE MEASURED.

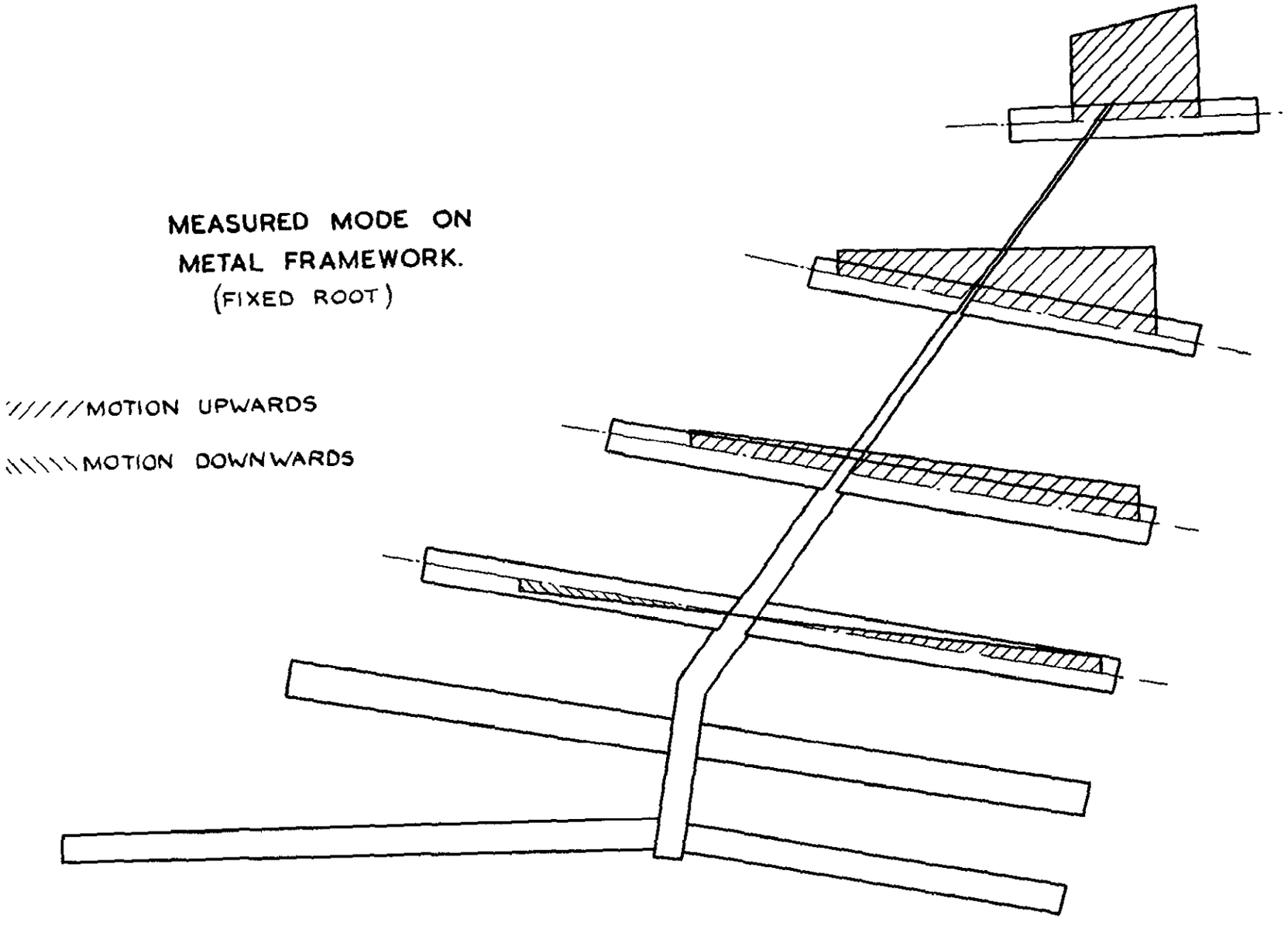

FIG. 8. MODE 1 ($f = 16.4$ c/s)

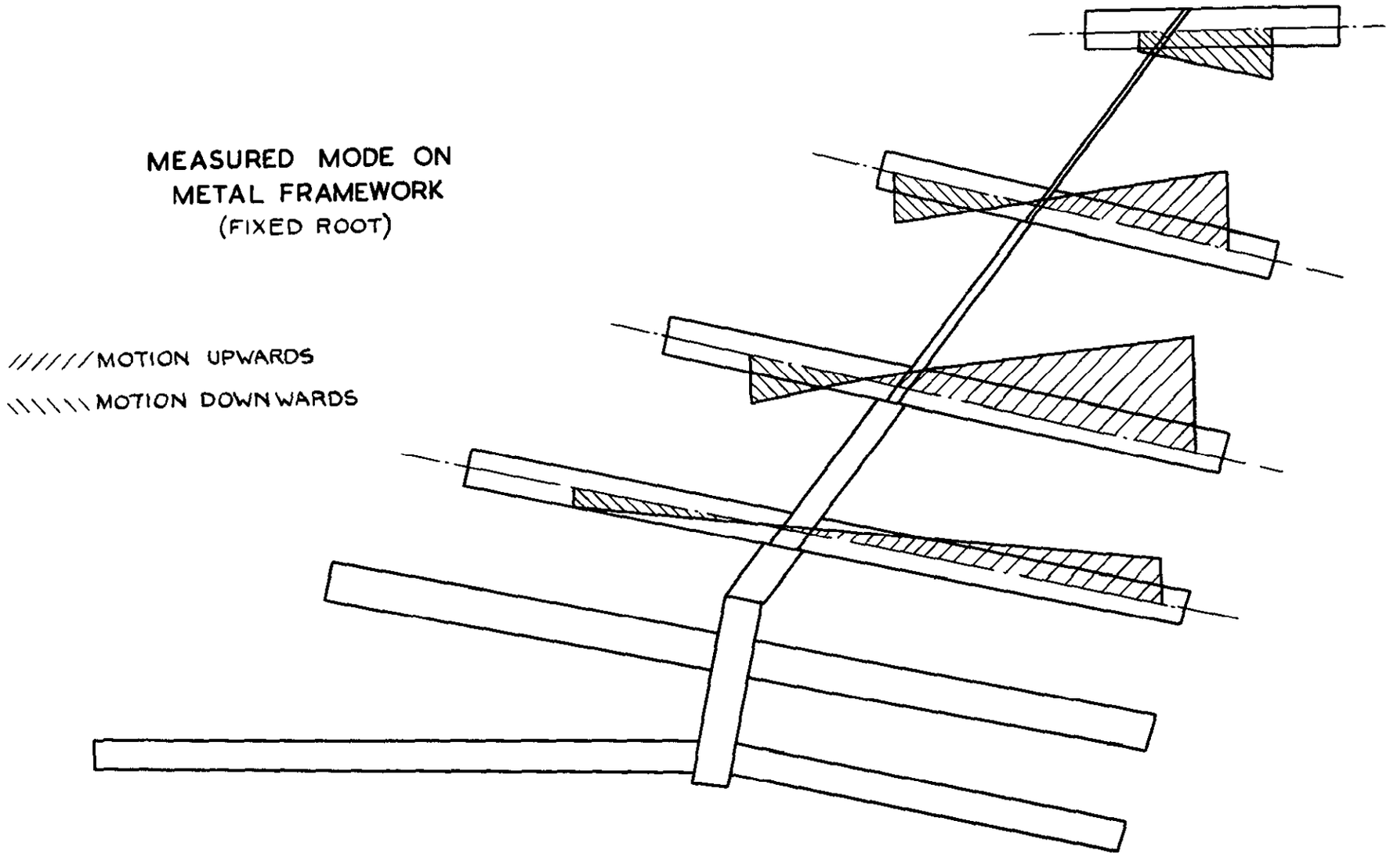

FIG. 9 MODE 2 ($f = 53.2$ c/s.)

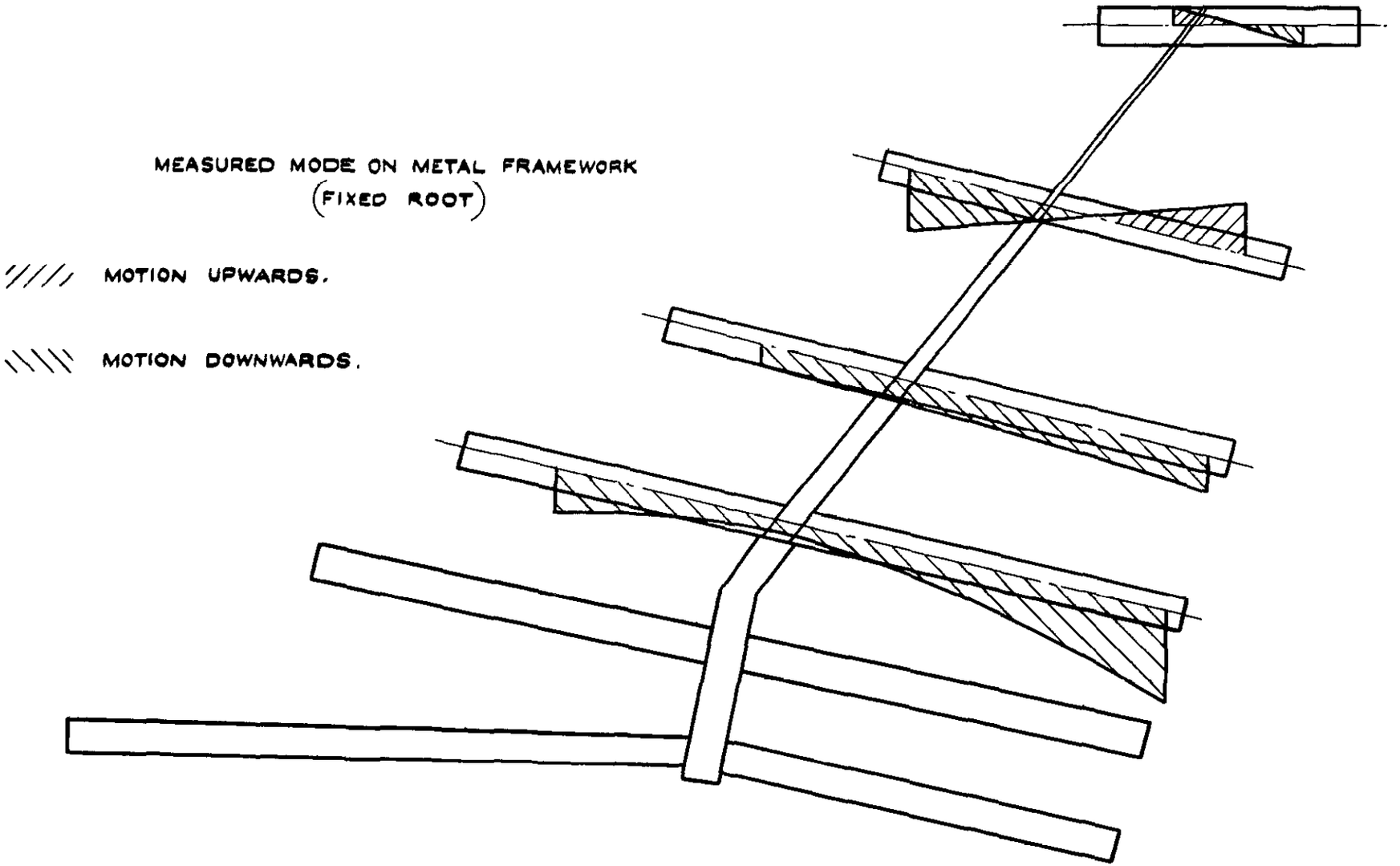

FIG. 10. MODE 3 ($f = 74 \cdot 2$ c/s)

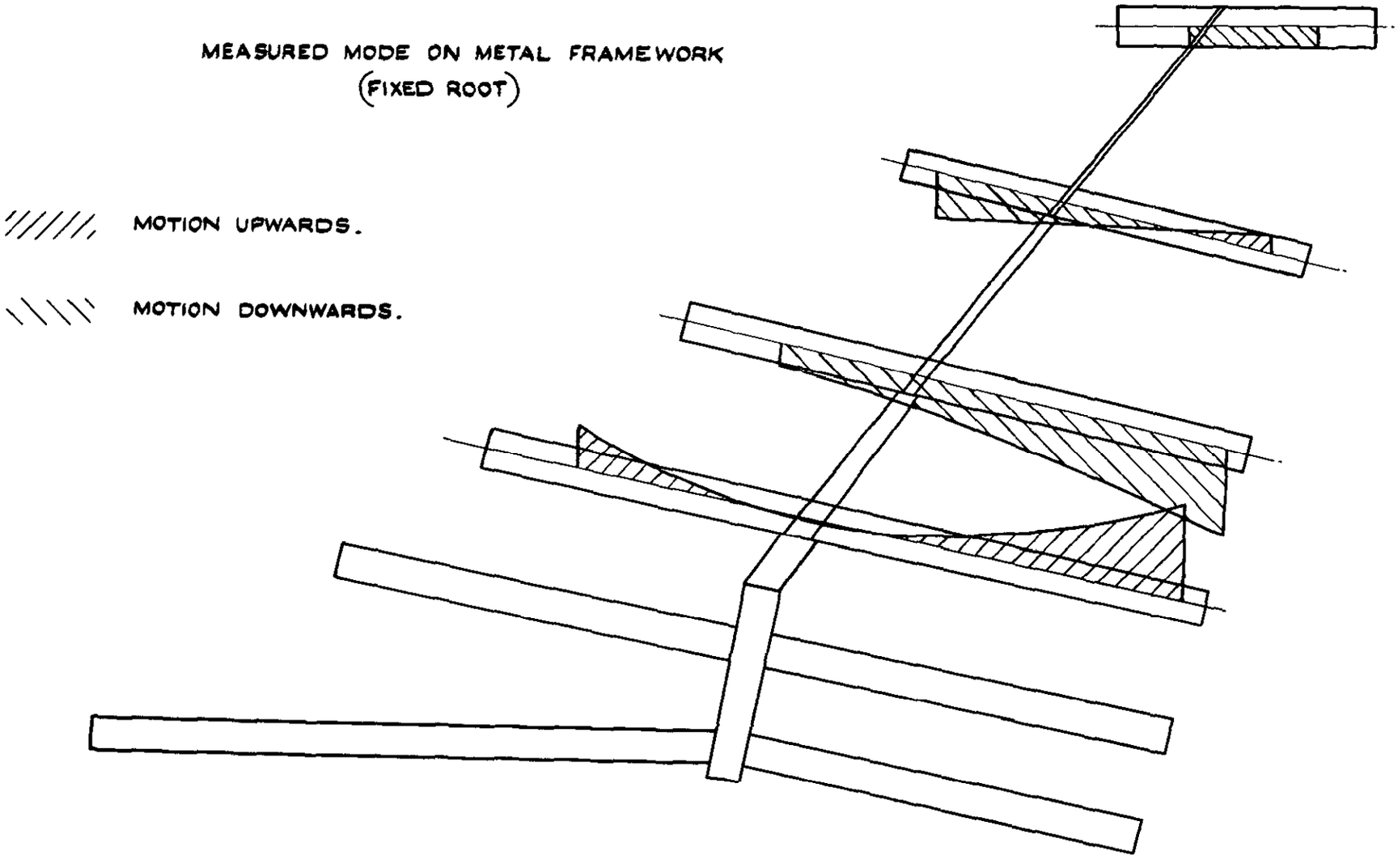

FIG. 11. MODE 4 (f = 87·0 c/s)

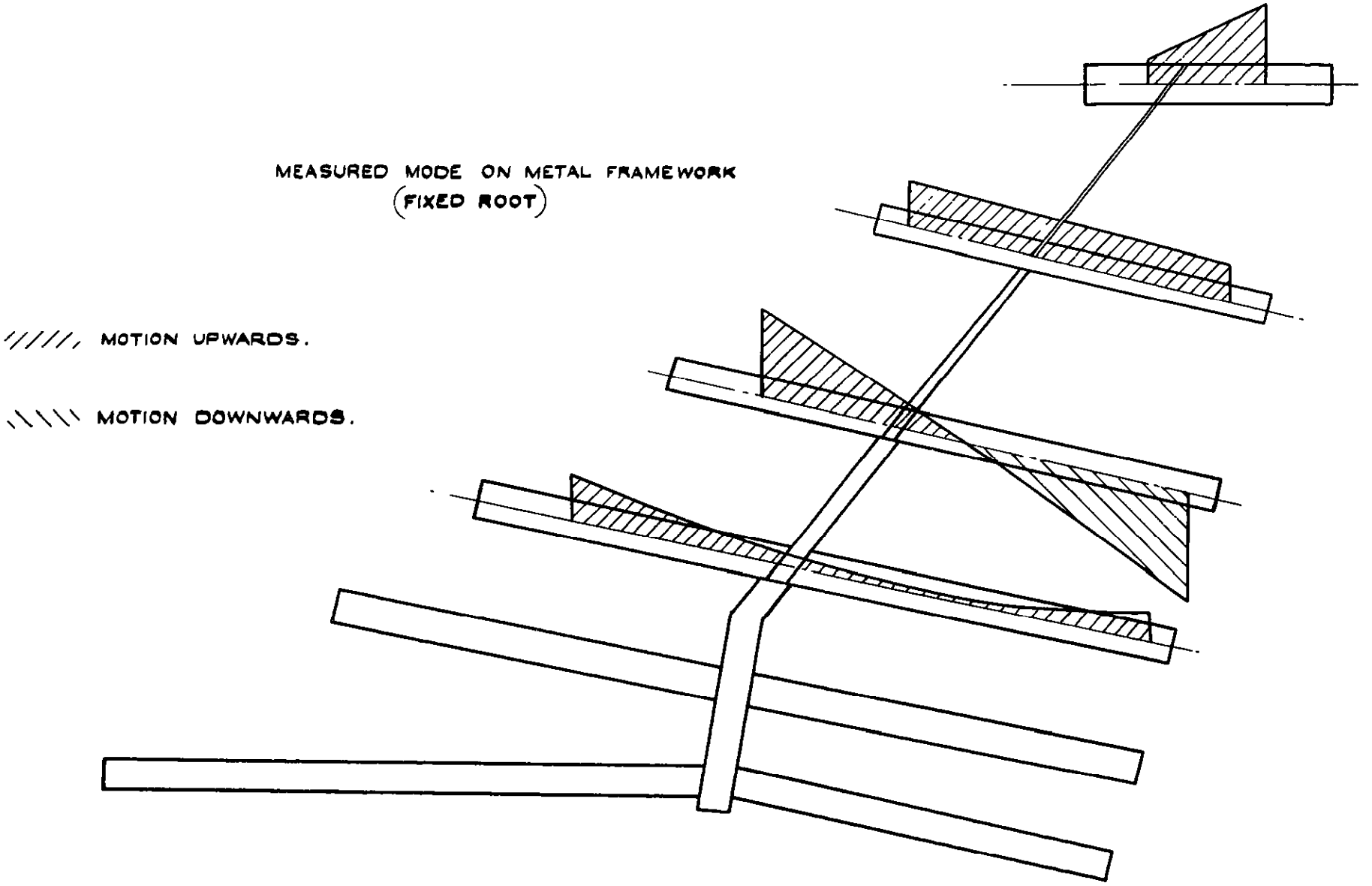

FIG. 12. MODE 5 (f = 102 c/s)

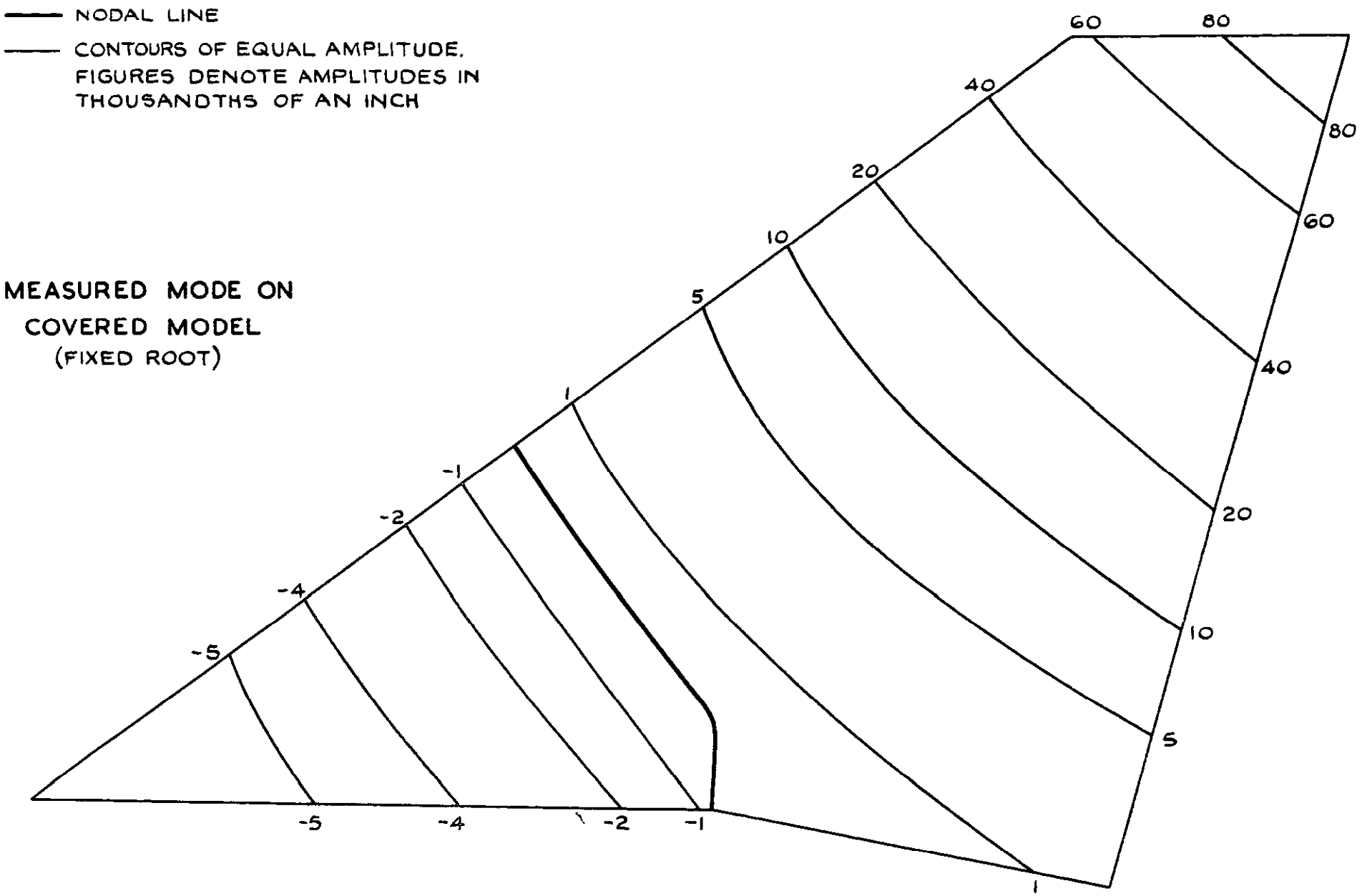

FIG. 13. MODE 1. (16·1 c/s)

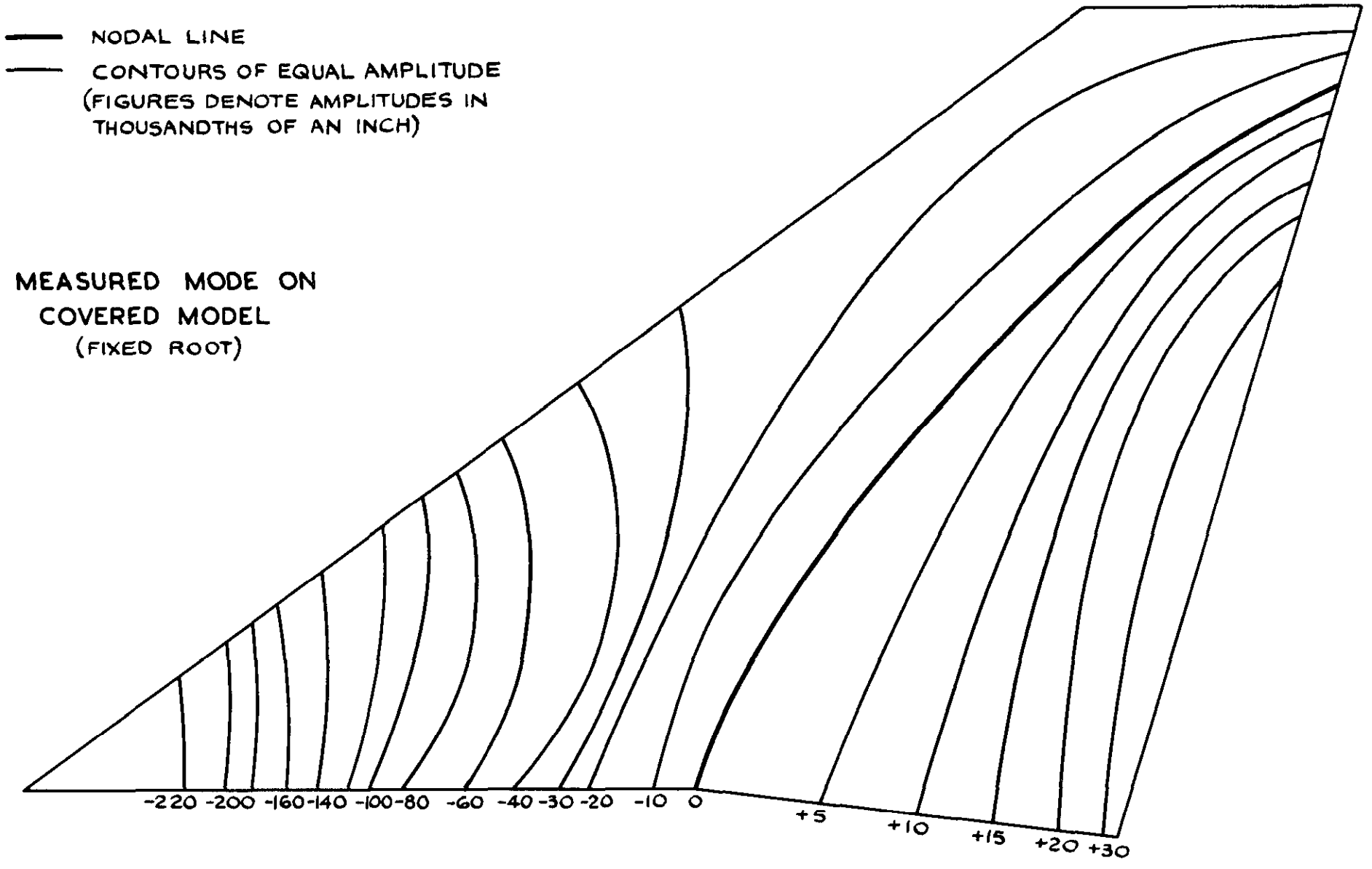

FIG. 14. MODE 2. (41 c/s)

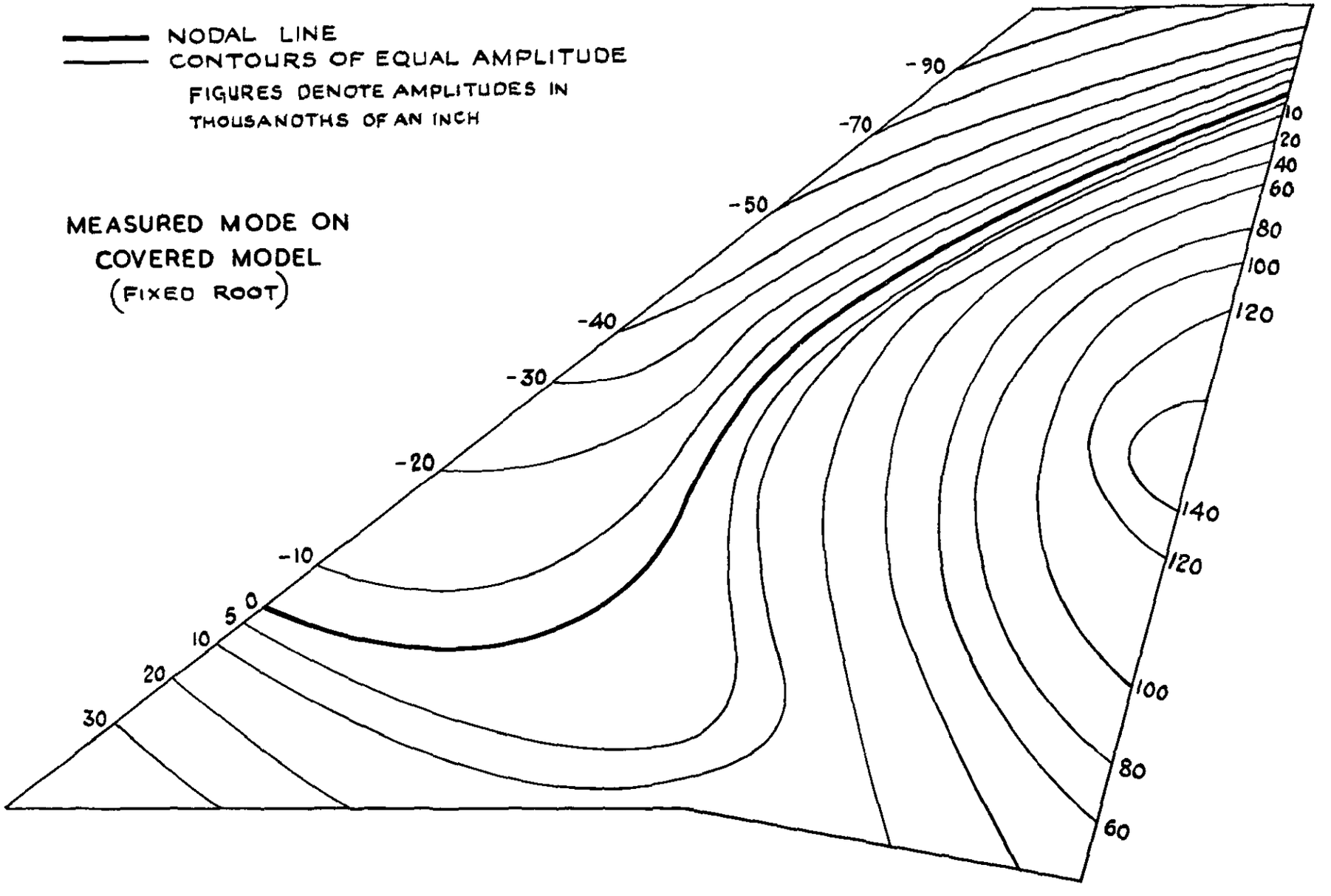

FIG. 15 MODEL 3 (54 c/s)

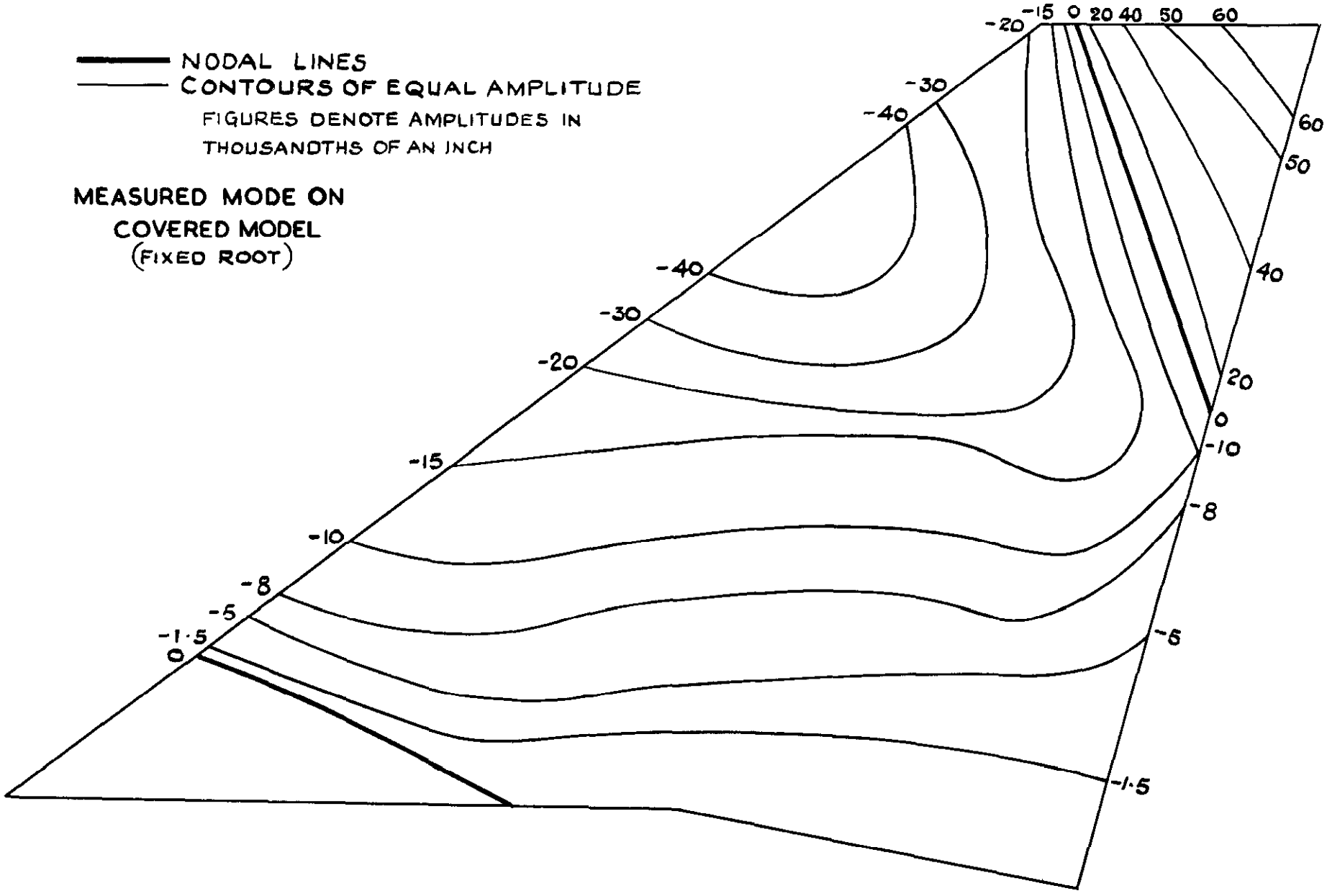

FIG 16 MODE 4 (64·8 c/s)

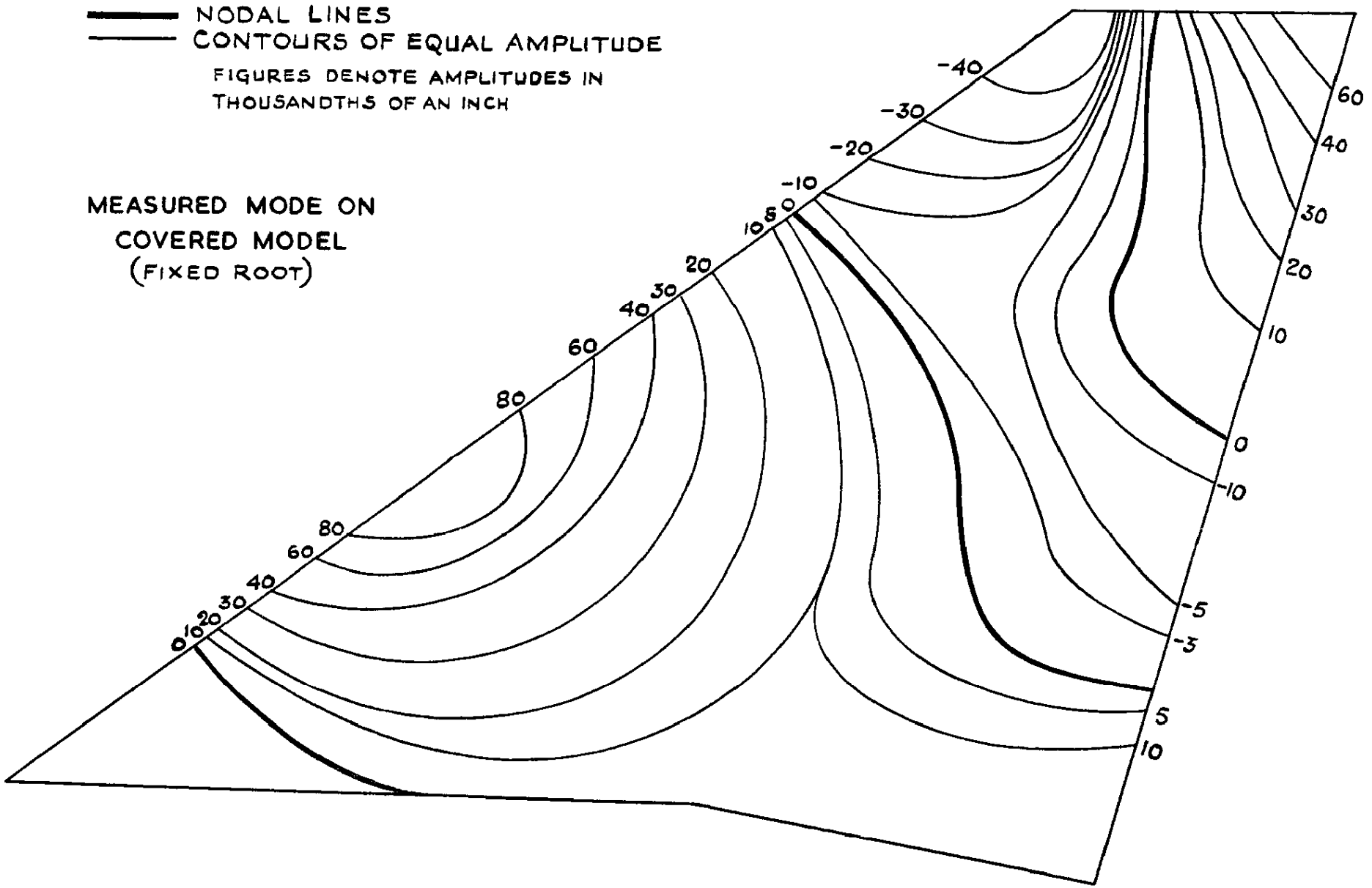

FIG. 17. MODEL 5 (109·8 c/s)

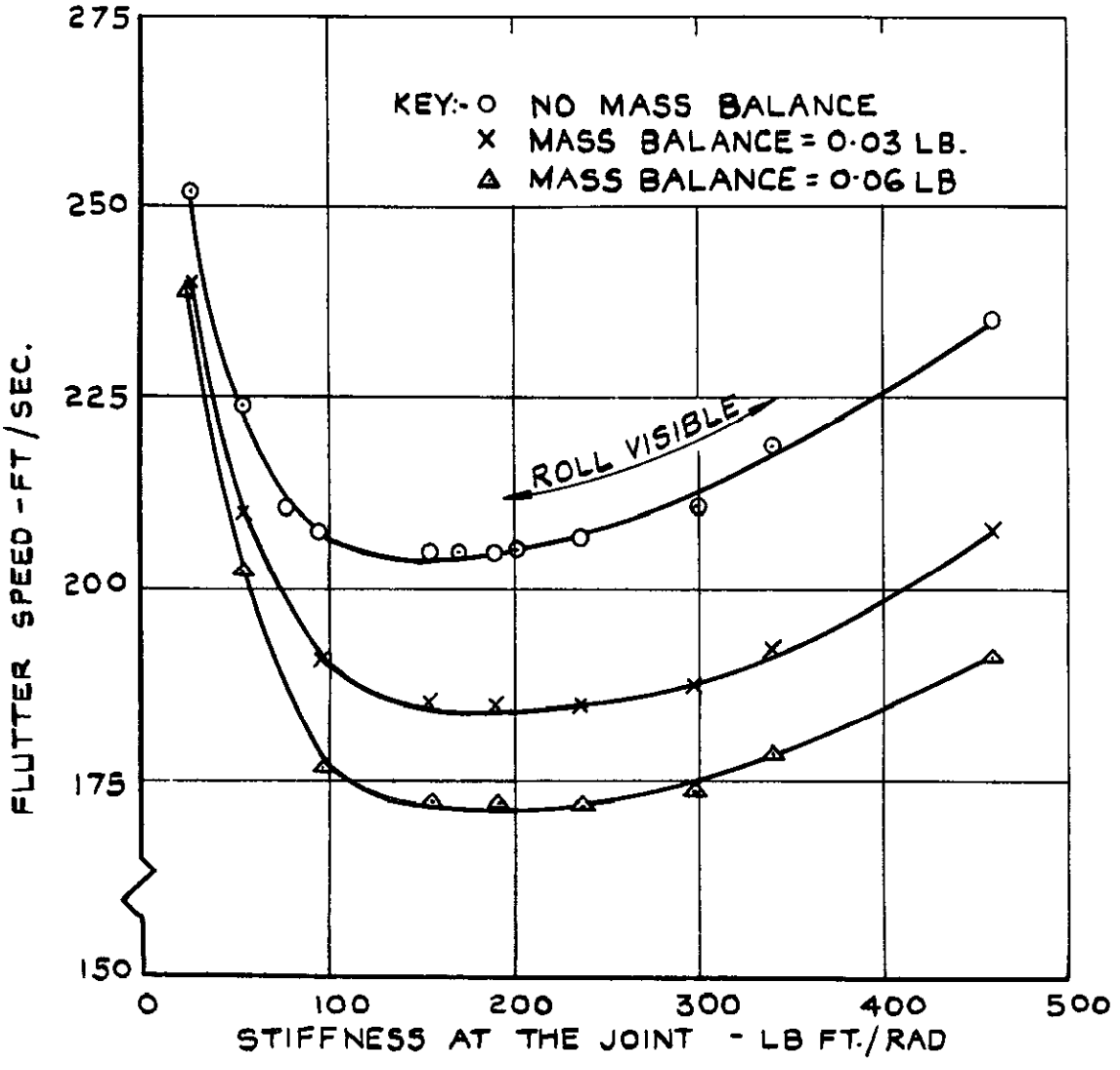

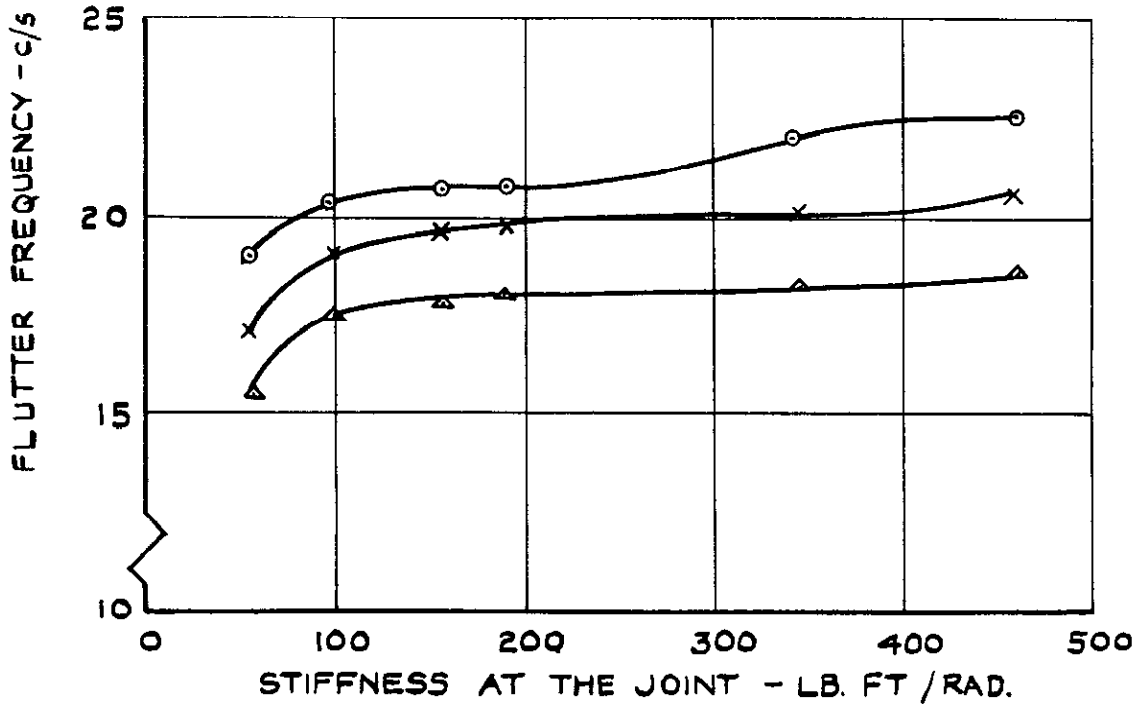

FIG. 18. RESULTS OF WIND TUNNEL TESTS.

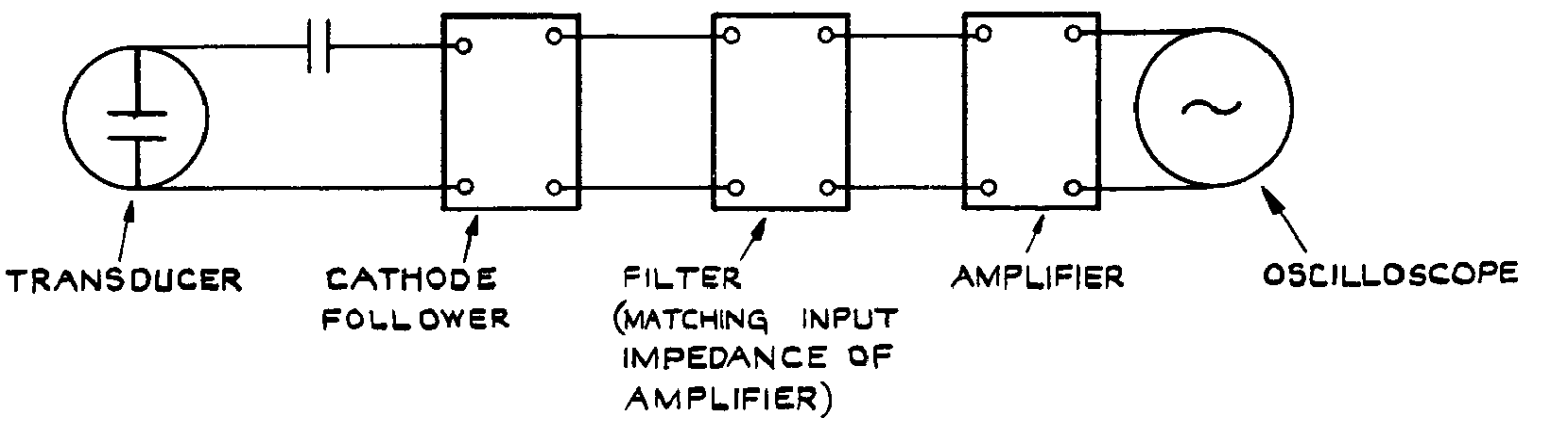

FIG. 19. TRANSDUCER AND ASSOCIATED EQUIPMENT.

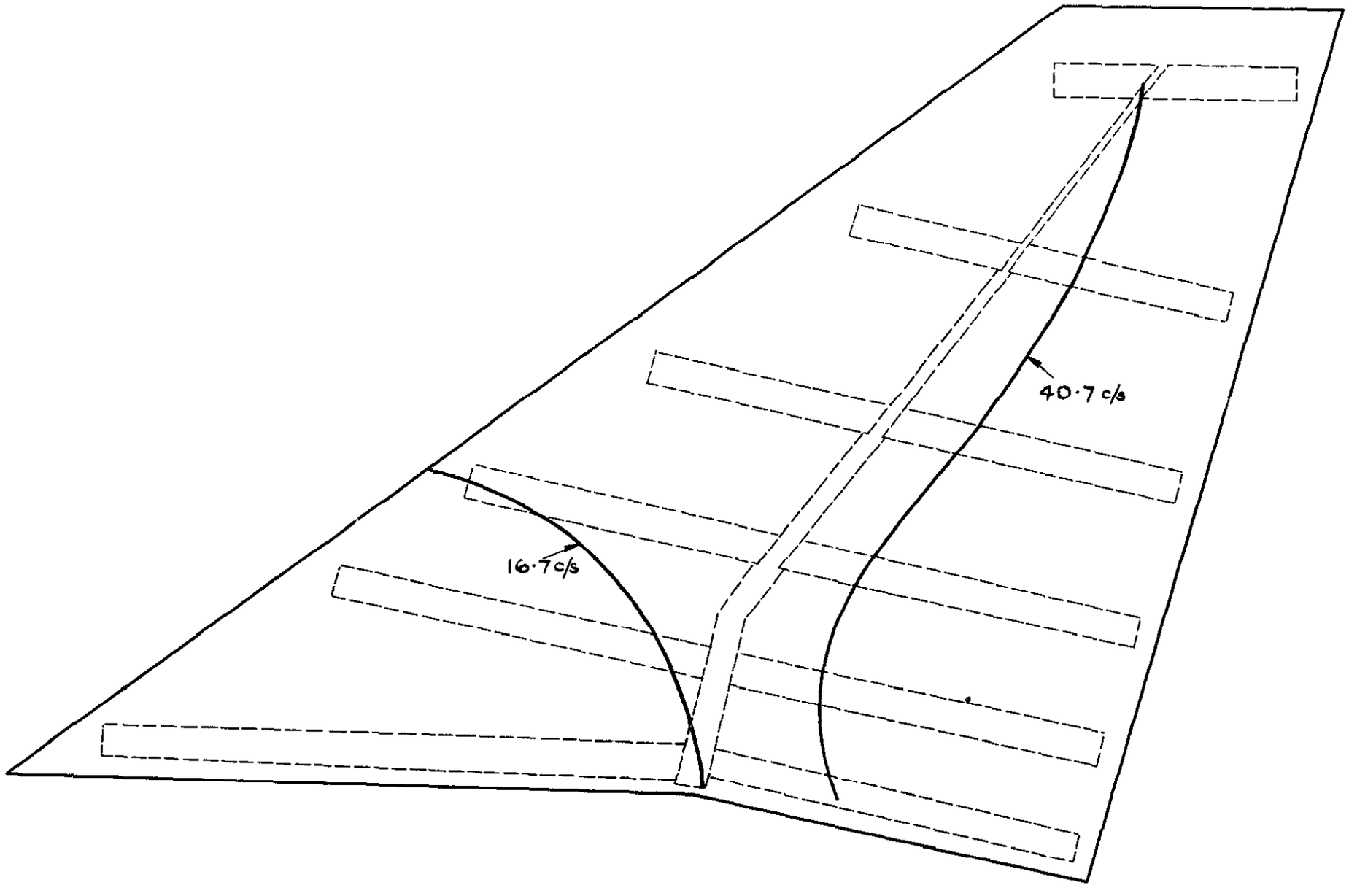

FIG.20. MODES 1 & 2 (CALCULATED)

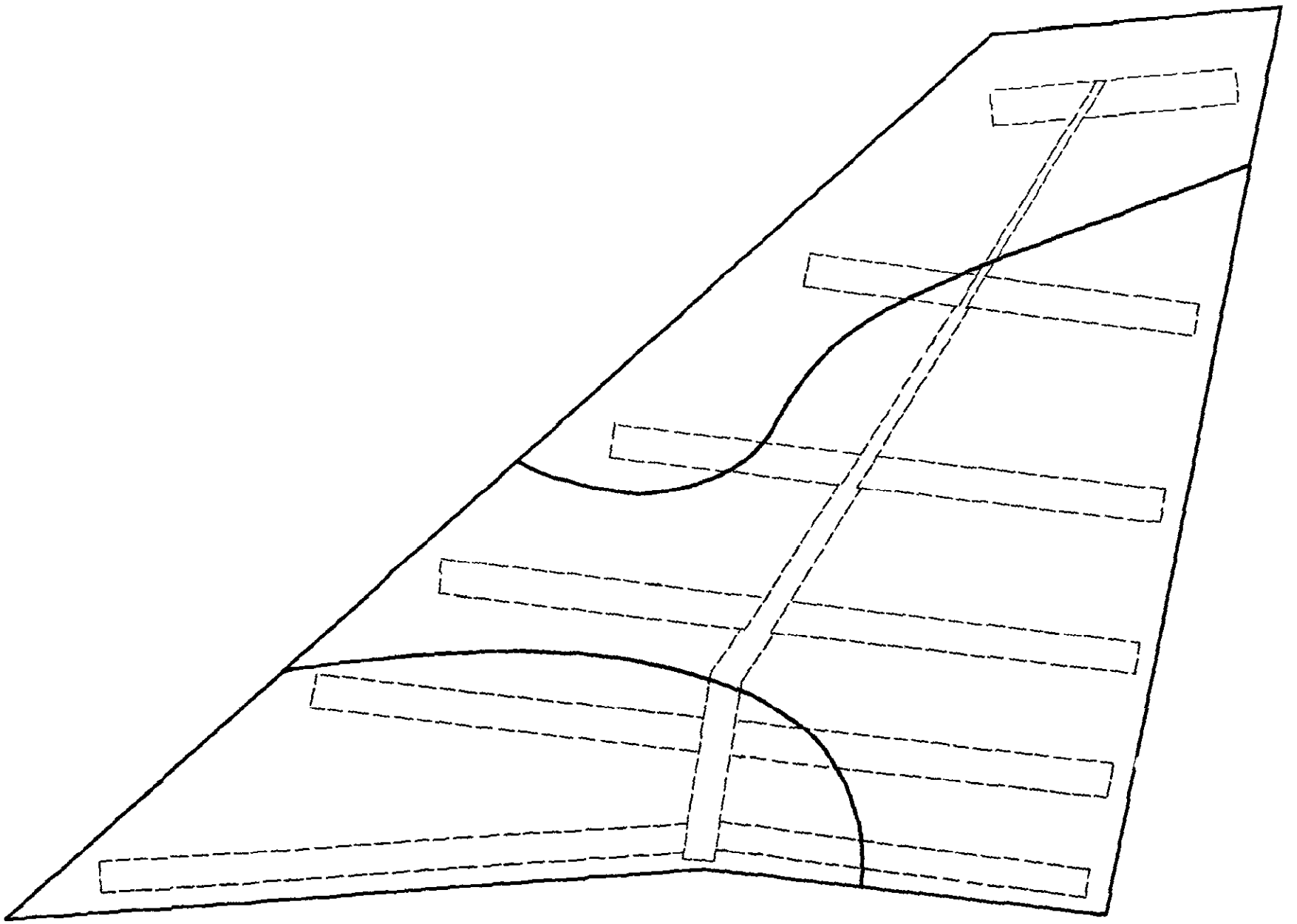

FIG.21. MODE 3 (CALCULATED) (48·74 c/s)

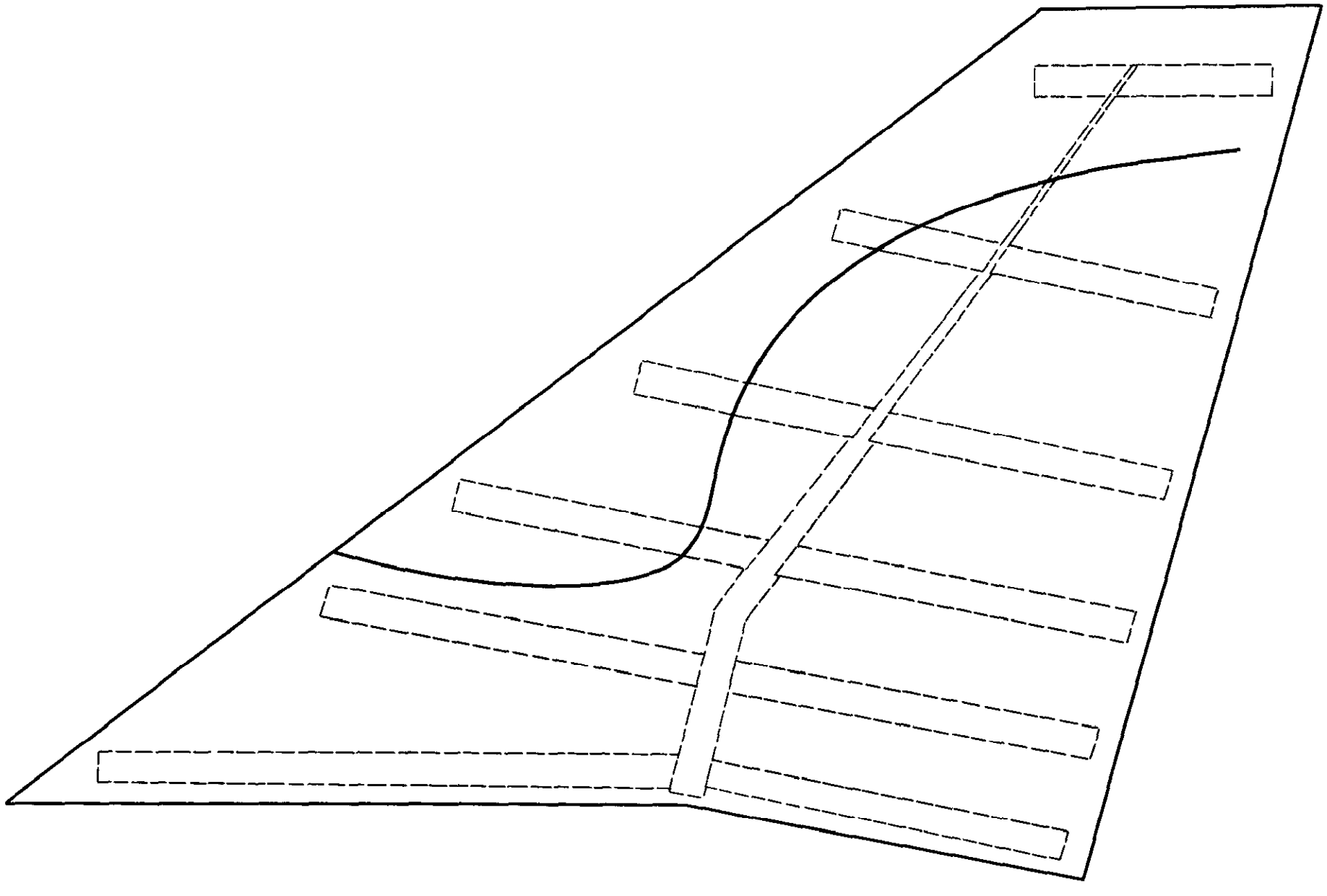

FIG.22. MODE 4 (CALCULATED) (53·4 c/s)

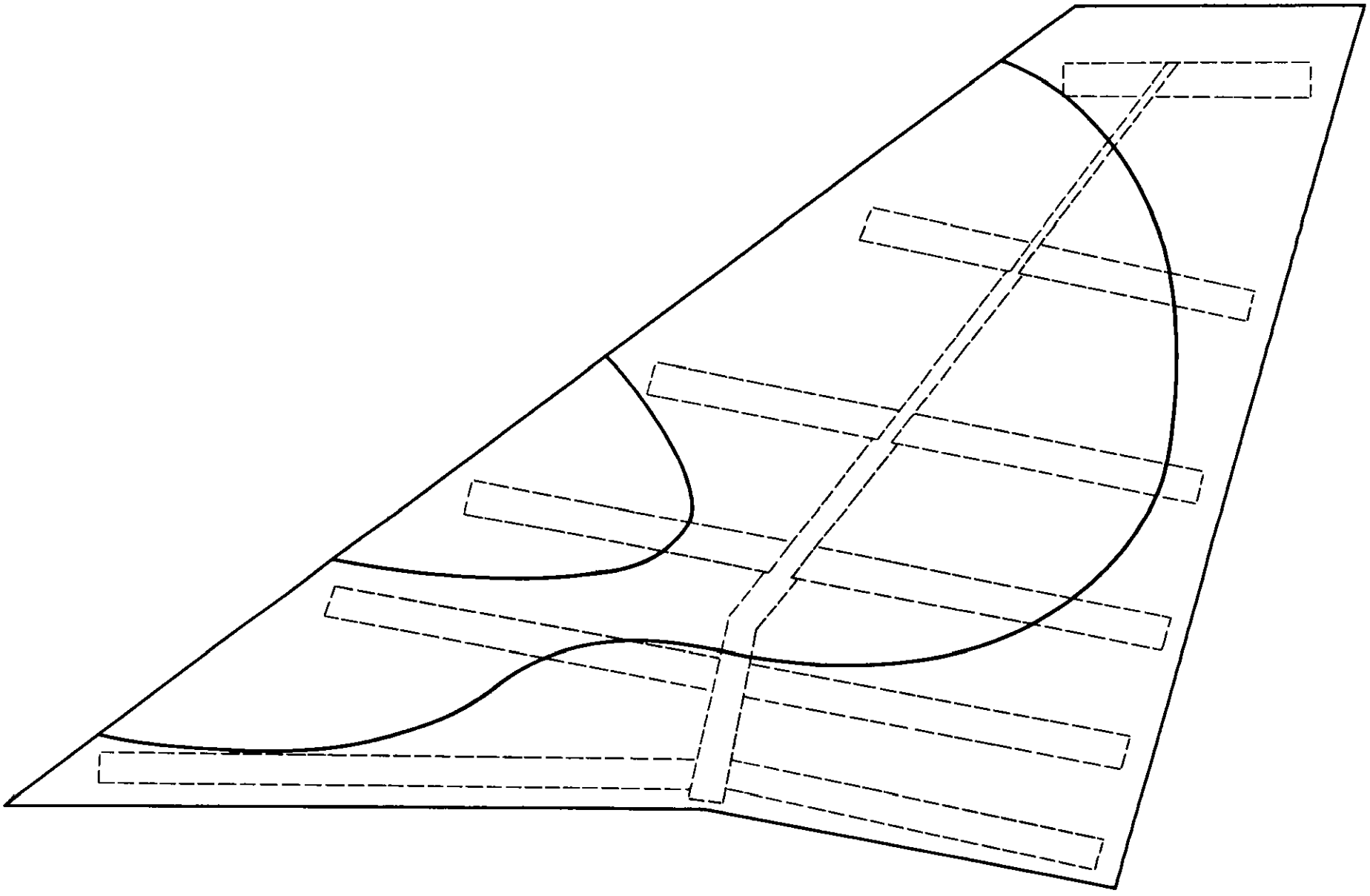

FIG.23. MODE 5 (CALCULATED.) (60·5 c/s)

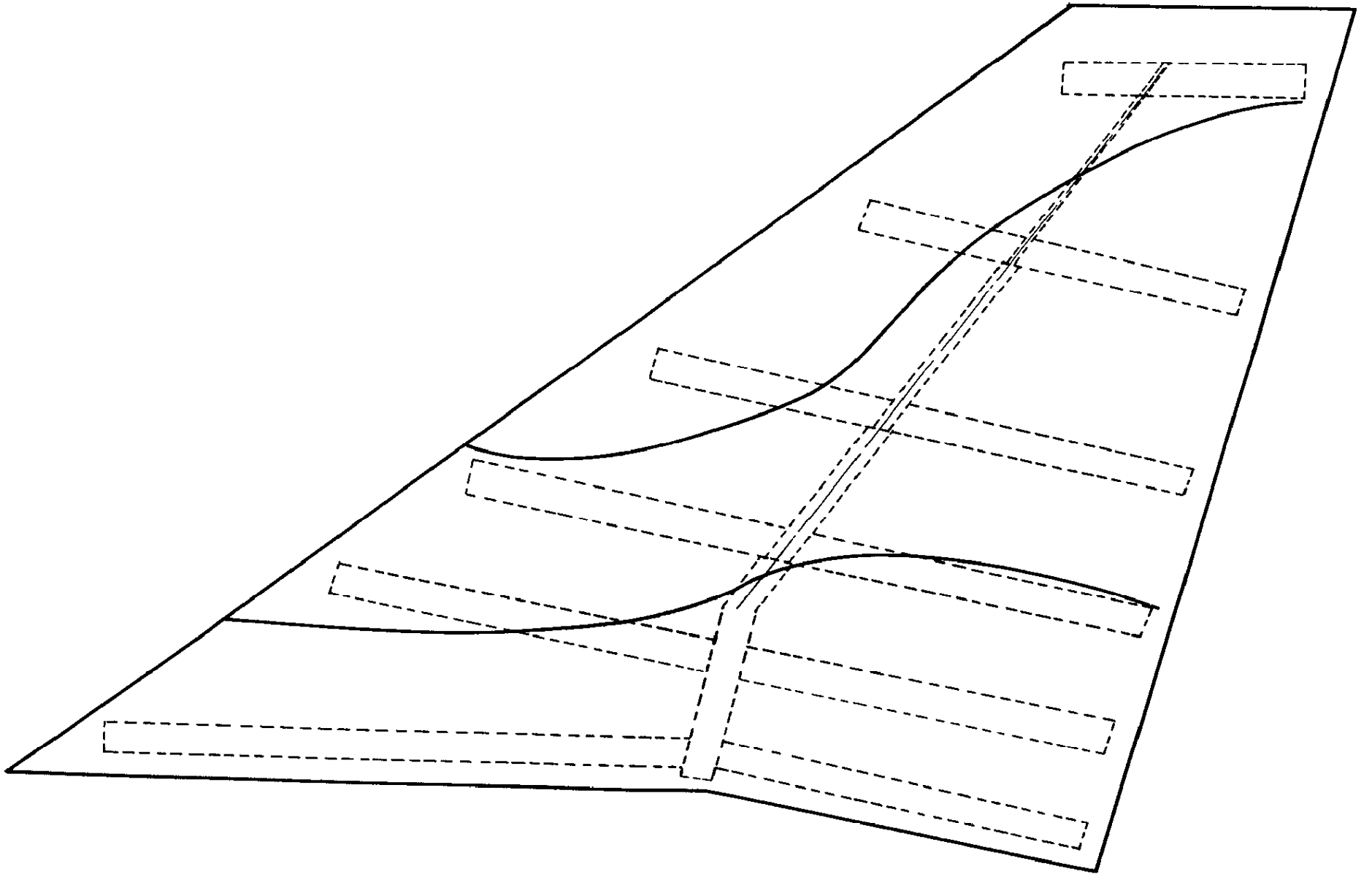

FIG. 24. MODE 6 (CALCULATED) (71·3 c/s)

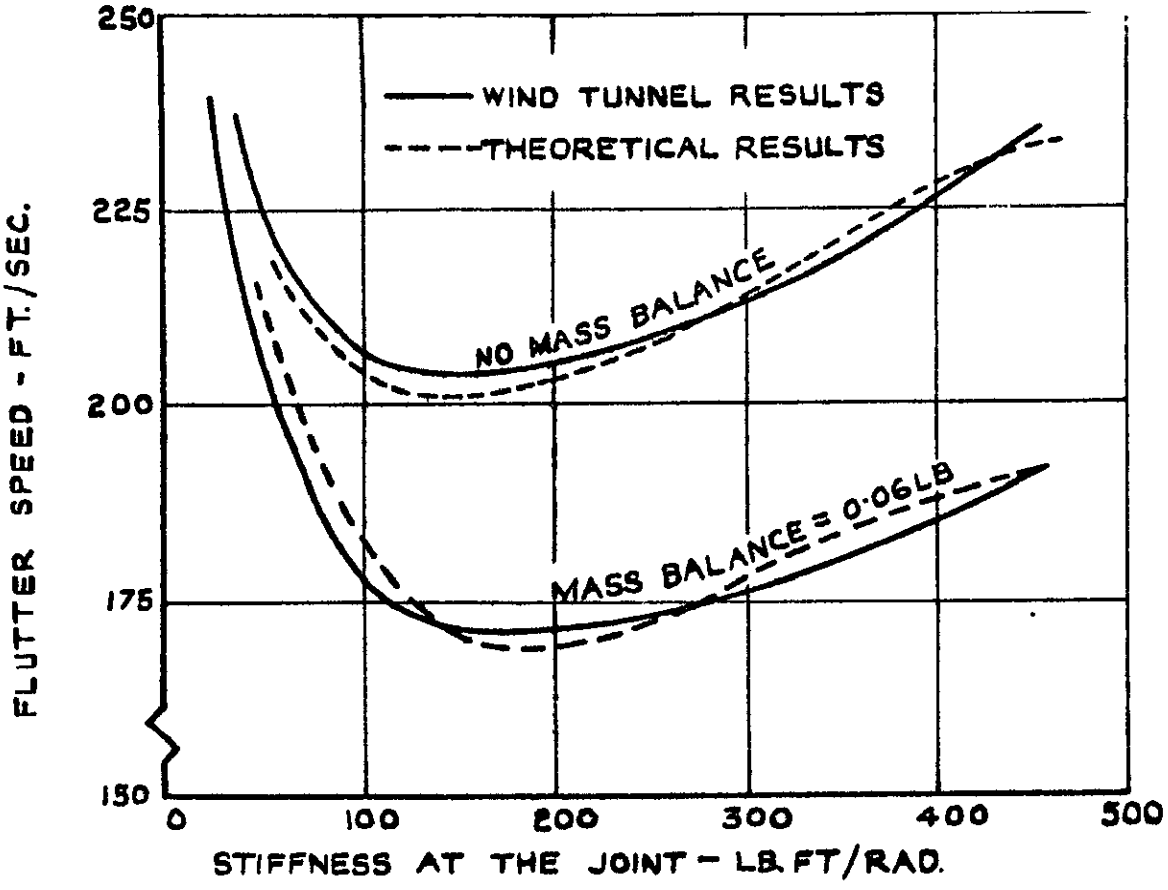

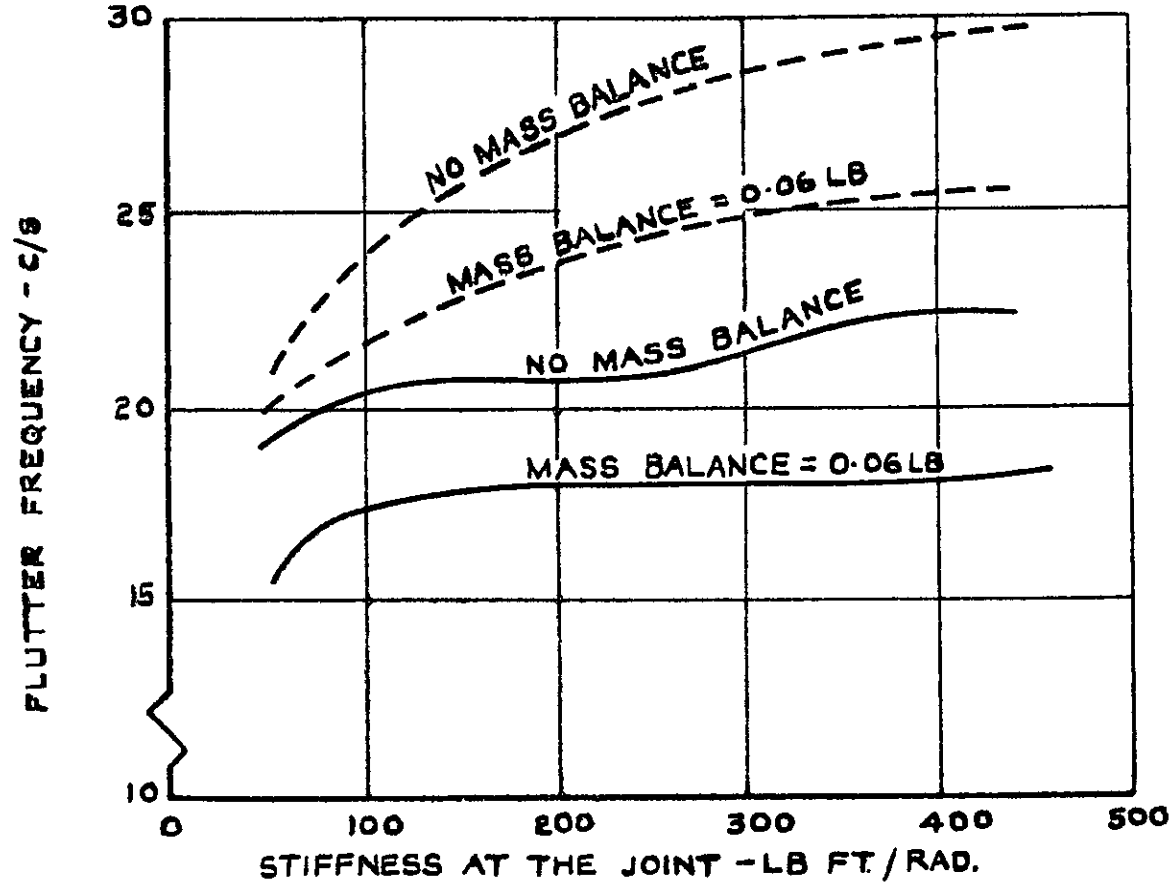

FIG. 25. COMPARISON OF EXPERIMENTAL AND THEORETICAL RESULTS

A.R.C. C.P. No.714

533.6.013.422 :
533.694.541

FLUTTER TESTS AND CALCULATIONS ON AN ALL-MOVING MODEL FIN.
Curran, J.K. July, 1963.

Low speed flutter tests have been made on an all-moving model fin to ascertain the effect of mass balance at a position on the leading edge near the root. The stiffness of the joint forming the roll axis for the model was also varied.

Good agreement is obtained between the experimental results and analytical predictions. As the stiffness at the joint is increased, allowing less freedom in roll, the flutter speed falls rapidly to a minimum, initially, and subsequently increases. Mass-balance reduces the flutter speeds and frequencies.

(Over)

A.R.C. C.P. No.714

533.6.013.422 :
533.694.541

FLUTTER TESTS AND CALCULATIONS ON AN ALL-MOVING MODEL FIN.
Curran, J.K. July, 1963.

Low speed flutter tests have been made on an all-moving model fin to ascertain the effect of mass balance at a position on the leading edge near the root. The stiffness of the joint forming the roll axis for the model was also varied.

Good agreement is obtained between the experimental results and analytical predictions. As the stiffness at the joint is increased, allowing less freedom in roll, the flutter speed falls rapidly to a minimum, initially, and subsequently increases. Mass-balance reduces the flutter speeds and frequencies.

(over)

A.R.C. C.P. No 714

533.6.013.422 :
533.694.541

FLUTTER TESTS AND CALCULATIONS ON AN ALL-MOVING MODEL FIN.
Curran, J.K. July, 1963.

Low speed flutter tests have been made on an all-moving model fin to ascertain the effect of mass balance at a position on the leading edge near the root. The stiffness of the joint forming the roll axis for the model was also varied.

Good agreement is obtained between the experimental results and analytical predictions. As the stiffness at the joint is increased, allowing less freedom in roll, the flutter speed falls rapidly to a minimum, initially, and subsequently increases. Mass-balance reduces the flutter speeds and frequencies.

(Over)

Calculations by the Aircraft Industry on a particular all-moving fin, which served as a basis for the model, gave the opposite effect for mass-balance, but the model did not accurately represent the chordwise flexibility of the actual fin and it is possible that the effectiveness of mass balance at the root depends on this parameter.

Calculations by the Aircraft Industry on a particular all-moving fin, which served as a basis for the model, gave the opposite effect for mass-balance, but the model did not accurately represent the chordwise flexibility of the actual fin and it is possible that the effectiveness of mass balance at the root depends on this parameter.

Calculations by the Aircraft Industry on a particular all-moving fin, which served as a basis for the model, gave the opposite effect for mass-balance, but the model did not accurately represent the chordwise flexibility of the actual fin and it is possible that the effectiveness of mass balance at the root depends on this parameter.

Published by
HER MAJESTY'S STATIONERY OFFICE
To be purchased from
York House, Kingsway, London, w.c.2
423 Oxford Street, London, w 1
13A Castle Street, Edinburgh 2
109 St Mary Street, Cardiff
39 King Street, Manchester 2
50 Fairfax Street, Bristol 1
35 Smallbrook, Ringway, Birmingham 5
80 Chichester Street, Belfast 1
or through any bookseller

C.P. No. 714

S O Code No 23-9015-14 K Ltd